

Dyson Equation Approach to Many–Body Greens Functions and Self–Consistent RPA First Application to the Hubbard Model

Steffen Schäfer^{1,2*}, Peter Schuck¹

¹ *Institut des Sciences Nucléaires, Université Joseph Fourier, CNRS–IN2P3
53, Avenue des Martyrs, F-38026 Grenoble Cedex, France*

² *Physik-Department T32, Technische Universität München
James-Franck-Straße 1, D-85747 Garching, Germany*

(November 26, 2024)

An approach for particle–hole correlation functions, based on the so-called SCRPA, is developed. This leads to a fully self–consistent RPA-like theory which satisfies the f –sum rule and several other theorems. As a first step, a simpler self–consistent approach, the renormalized RPA, is solved numerically in the one–dimensional Hubbard model. The charge and the longitudinal spin susceptibility, the momentum distribution and several ground state properties are calculated and compared with the exact results. Especially at half filling, our approach provides quite promising results and matches the exact behaviour apart from a general prefactor. The strong coupling limit of our approach can be described analytically.

PACS numbers:71.10.-w, 75.10.Jm, 72.15.Nj

I. INTRODUCTION

The advent of high T_c super–conductivity, which remains unexplained theoretically in its essence, has spurred an enormous quest for developing many–body approaches capable to describe strongly correlated Fermion systems. Various formalisms have been applied in the past, each with its strengths and deficiencies (for a review see ref.¹).

However, contrary to standard mean–field theory which is a commonly accepted lowest–order many–body approach, for correlation functions, such a generic method is missing so far. In this respect, any new and promising vistas are worthwhile to be pursued and elaborated. Indeed, in the recent past, a theory for two–body correlation functions has been developed bearing the characteristics of a generalization of Hartree–Fock theory to two–body clusters. In its roots this theory goes back rather far in time and has been promoted independently by several groups^{2–5}. In the literature, it is known under various names such as Self–Consistent RPA (SCRPA), Cluster Mean Field (CMF) and Equation of Motion Method (EOM)^{2–5}. In itself it is an approximation to the so-called Dyson Equation Approach (DEA) to correlation functions where one replaces the full mass operator by its instantaneous part. However, only recently this method has found the attention and formal developments it deserves with, indeed, very promising results. The most outstanding of those is certainly the exact reproduction of the lowest spin–wave excitation spectrum, $\omega_k = \frac{\pi}{2} |\sin k|$, known from the Bethe ansatz, of the antiferromagnetic Heisenberg chain⁶. Moreover, also some simpler models have been treated successfully in this approach⁷. Encouraged by these results, we thought it worthwhile to apply the method to the strongly correlated electron problem within the single–band Hubbard Hamiltonian with on–site repulsion U .

Since the approach, which we hitherto want to call SCRPA, is based on non–linear equations for non–local two–body correlation functions, one understands that it is numerically very demanding. We therefore choose as a first application the one–dimensional Hubbard model for several reasons:

- The exact solution of the ground state is known from the Bethe ansatz⁸. Therefore, a direct comparison of the SCRPA results is possible.
- The numerical effort in one dimension may be expected to be more modest than in higher dimensions.
- The experience gained in the $1d$ case may help us to attack higher dimensions in the future.

*email: steffen@in2p3.fr

The price to pay for this strategy is that one-dimensional problems are notoriously difficult to describe because of their extreme quantum character. As our method is not specifically designed for one dimension, we cannot expect it to reproduce particularities, such as Luttinger liquid behaviour.

As we will see, our approach nonetheless permits to obtain interesting results in one dimension. They should, however, be judged in the light that in this first application to the Hubbard model we did not solve the SCRPA equations in full but applied a rather obvious and from the numerical point of view very simplifying approximation. Nevertheless, this approximation, known in the literature under the name of renormalized RPA, keeps the essentials of the self-consistency aspects.

We demonstrate in this paper that the formalism allows for the self-consistent solution of a fully closed system of non-linear equations for two-body correlation functions. Moreover, important formal theorems are respected. Among those, we, for instance, cite the fulfillment of the f -sum rule (energy weighted sum rule) and of the Luttinger theorem.

Other interesting results concern the strong coupling regime of the half filled chain. For example, the self-consistently calculated momentum distribution can be found analytically in the large U limit. It obeys $n_k \propto \cos k$ with a proportionality factor of $4/U$ instead of $8 \ln 2/U$ of the exact result, known from the large U expansion of the Bethe ansatz solution, resulting in an error smaller than 30%. This result is the more astonishing as it was obtained with the renormalized RPA approach. It can be expected that it will be substantially improved once the full SCRPA solution is available.

The paper is organized as follows. In section II, in order to make our paper self-contained, we will give a brief overview of the SCRPA theory starting from the equation of motion for a completely general Green's function. In particular, the explicit form of the self-consistent and renormalized RPA particle-hole propagators is derived in terms of a closed system of non-linear self-consistent equations. In section III, our approach is applied to charge and spin correlation functions in the Hubbard model. In section IV, we solve numerically the set of self-consistent equations for the renormalized RPA response functions for different fillings and interaction strengths. Our results are compared with the Bethe ansatz solution and with Quantum Monte Carlo calculations. For half filling and large U , analytic expressions are given for the momentum distribution function and the susceptibilities of our theory. In section V, we draw some conclusions and give an outlook on some improvements which are planned to be implemented in our approach. In appendix A, we outline the connection between the SCRPA and a variational ansatz which minimizes the energy weighted sum rule. Appendix B provides the explicit expressions for the free particle-hole susceptibility in one dimension. In appendix C, we show how the analytic expressions which we derived for the strong coupling limit of our theory at half filling, are a rigorous solution of the renormalized RPA equations.

II. THE DYSON EQUATION APPROACH TO MANY-BODY GREEN'S FUNCTIONS

In this section, we briefly want to review the Dyson Equation Approach (DEA) to correlation functions⁹. The DEA is increasingly used in the many-body community and has recently produced interesting results in various domains of many-body physics⁴⁻⁷.

Let us start with the definition of a general causal (time ordered) or retarded many-body Green's function at zero temperature and at equilibrium (the generalization to finite temperature, using the Matsubara technique, is straightforward),

$$\begin{aligned} G_{AB}^c(t, t') &\equiv \langle\langle A(t); B(t') \rangle\rangle^c \\ &:= -i \langle 0 | T_\epsilon A(t) B(t') | 0 \rangle \end{aligned} \quad (1)$$

$$\begin{aligned} G_{AB}^{\text{ret}}(t, t') &\equiv \langle\langle A(t); B(t') \rangle\rangle^{\text{ret}} \\ &:= -i \Theta(t - t') \langle 0 | [A(t), B(t')]_{-\epsilon} | 0 \rangle, \end{aligned} \quad (2)$$

where $|0\rangle$ is the exact ground-state and T_ϵ Wick's time-ordering operator.

Here, $A(t)$ and $B(t')$ are arbitrary operators built out of any number of annihilation and/or creation operators of Bosons or Fermions or mixtures of both. Usually A and B will depend on one or several indices, and the notation $\langle\langle A; B \rangle\rangle$ has to be considered as a shorthand for the matrix Green's function $\langle\langle A_\alpha; B_\beta \rangle\rangle$ where α and β run over the whole set of quantum numbers. The operators A and B can also be spin operators or even more general operators such as multi-component operators $\mathbf{A} = (A_1, A_2, \dots)$ where the single components are again chosen according to the problem in question. For the derivation of a Dyson equation, however, we will choose $B = A^+$. The case $B \neq A^+$ needs further considerations which may be important for the derivation of integral equations for vertex functions.

The time dependence of the operators is given in the Heisenberg picture, $X(t) = e^{iHt} X e^{-iHt}$, where the Hamiltonian H is also completely general. It may describe relativistic or non-relativistic Fermi, Bose or spin systems or any system for which a Hamilton operator exists.

At equilibrium the two time Green's functions (1) depend only on the time difference such that their Fourier transforms are only functions of one frequency. These are the quantities for which we want to derive a Dyson equation. As the derivation is the same for either causal or retarded Green's functions we will from now on omit the upper indices.

Let us establish the equation of motion for $G_{AB}(t, t')$:

$$i \frac{\partial}{\partial t} \langle\langle A(t); B(t') \rangle\rangle = \delta(t - t') \langle [A, B]_{-\epsilon} \rangle + \langle\langle [A, H](t); B(t') \rangle\rangle, \quad (3)$$

or, in energy representation,

$$\omega \langle\langle A; B \rangle\rangle_{\omega} = \langle [A, B]_{-\epsilon} \rangle + \langle\langle [A, H]; B \rangle\rangle_{\omega}. \quad (4)$$

On the rhs of (4) the commutator

$$\mathcal{N} := \langle [A, B]_{-\epsilon} \rangle \quad (5)$$

plays the role of a norm matrix, and $\langle\langle [A, H]; B \rangle\rangle_{\omega}$ is a general Green's function containing the interaction once explicitly. For fermion like operators A and B we will use the anti-commutator Green's function ($\epsilon = -$) and for boson like (e.g. a product of an even number of fermion operators) the commutator Green's function ($\epsilon = +$).

Under the assumption that the inverse of $\langle\langle A; B \rangle\rangle_{\omega}$ exists, an effective ‘‘Hamiltonian’’ $\mathcal{H}_{AB}(\omega)$ can be defined as

$$\mathcal{H}_{AB}(\omega) = \langle\langle [A, H]; B \rangle\rangle_{\omega} \langle\langle A; B \rangle\rangle_{\omega}^{-1}. \quad (6)$$

The equation of motion (4) can thus be transformed into a Dyson equation,

$$\omega \langle\langle A; B \rangle\rangle_{\omega} = \mathcal{N} + \mathcal{H}_{AB}(\omega) \langle\langle A; B \rangle\rangle_{\omega}. \quad (7)$$

We stress again that the products on the rhs. of eqs. (6) and (7) are understood to be matrix multiplications.

As we do not yet know how to determine the effective Hamiltonian $\mathcal{H}_{AB}(\omega)$, the solution of the Dyson eq. (7),

$$\langle\langle A; B \rangle\rangle_{\omega} = \left\{ \omega - \mathcal{H}_{AB}(\omega) \right\}^{-1} \mathcal{N}, \quad (8)$$

remains for the moment completely formal. In order to derive a more explicit and useful expression for $\mathcal{H}_{AB}(\omega)$, we insert the inverse of the formal solution (8) in (6):

$$\begin{aligned} \mathcal{H}_{AB}(\omega) &= \langle\langle [A, H]; B \rangle\rangle_{\omega} \mathcal{N}^{-1} \left\{ \omega - \mathcal{H}_{AB}(\omega) \right\} \\ &\equiv \mathcal{H}_{AB}^I(\omega) - \mathcal{H}_{AB}^{II}(\omega) \end{aligned} \quad (9)$$

The first part, $\mathcal{H}_{AB}^I(\omega) \equiv \langle\langle [A, H]; B \rangle\rangle_{\omega} \mathcal{N}^{-1}$, can be obtained from the equation of motion for the higher Green's function $\langle\langle [A, H]; B \rangle\rangle_{\omega}$ which is set up from ‘‘the right’’ this time (i.e. deriving with respect to t' instead of t):

$$\langle\langle [A, H]; B \rangle\rangle_{\omega} = \langle [A, H], B \rangle_{-\epsilon} + \langle\langle [A, H]; [H, B] \rangle\rangle_{\omega} \quad (10)$$

If we adopt $B \equiv A^+$, the second part of the effective Hamiltonian, $\mathcal{H}_{AB}^{II}(\omega) \equiv \langle\langle [A, H]; B \rangle\rangle_{\omega} \mathcal{N}^{-1} \mathcal{H}_{AB}(\omega)$, contains only n -line *reducible* contributions¹⁰, with n being the number of fermion operators in A . Further, it can be shown¹⁰ that the sole function of $\mathcal{H}_{AB}^{II}(\omega)$ is to cancel *all* reducible contributions of $\mathcal{H}_{AB}^I(\omega)$. As the double commutator $\langle [A, H], B \rangle_{-\epsilon}$ has no reducible contributions, we just have to put an index ‘‘irreducible’’ on the Green's function on the rhs. of eq. (10) to obtain as the final expression for the effective Hamiltonian:

$$\begin{aligned} \mathcal{H}_{AB}(\omega) &= \left\{ \langle [A, H], B \rangle_{-\epsilon} + \langle\langle [A, H]; [H, B] \rangle\rangle_{\omega}^{\text{irr}} \right\} \mathcal{N}^{-1} \\ &\equiv \mathcal{H}_{AB}^{\text{SC}} + \mathcal{H}_{AB}^{\text{res}}(\omega) \end{aligned} \quad (11)$$

We see that the effective Hamiltonian (11) splits up in a natural way in an instantaneous part and in a truly dynamic (resonant) part. The latter contains scattering processes leading to imaginary potentials and corresponding real ones with a frequency dependence.

To obtain a better understanding of the various terms contributing to the effective Hamiltonian, let us analyze eq. (11) for the well-known case of the single-particle propagator, that is $A = a_1$ and $B = a_1^\dagger$. Since later we want to restrict ourselves to a non-relativistic fermion system let us consider a typical Hamiltonian

$$H = \sum_{12} t_{12} a_1^\dagger a_2 + \frac{1}{4} \sum_{1234} \bar{v}_{1234} a_1^\dagger a_2^\dagger a_4 a_3 \quad (12)$$

where a, a^\dagger are fermion destruction and creation operators. The matrix elements t_{12} and $\bar{v}_{1234} = v_{1234} - v_{1243}$ of the kinetic energy and the two-particle interaction, respectively, are expressed in an arbitrary single-particle basis which comprises for example quantum numbers for momentum, spin, isospin, and so on.

The norm matrix (5) is thus given by $\mathcal{N}_{11'} = \delta_{11'}$. In this case, the effective Hamiltonian is the sum of the single-particle energy and the full self-energy. The static part of the effective Hamiltonian, expressed by the double commutator $\langle [[a_1, H], a_1^\dagger]_+ \rangle$, yields the Hartree-Fock or mean-field Hamiltonian. We thus have recovered an important piece of the single-particle Dyson equation. Working out the second part of the effective Hamiltonian in eq. (11) yields the following $2p - 1h$ Green's function:

$$\frac{1}{4} \sum_{\substack{234 \\ 2'3'4'}} \bar{v}_{1234} \langle\langle (a_2^\dagger a_4 a_3)_t; (a_{3'}^\dagger a_{4'}^\dagger a_{2'})_{t'} \rangle\rangle_\omega^{\text{irr}} \bar{v}_{4'3'2'1'} . \quad (13)$$

As mentioned above, in eq. (13), all reducible contributions to the effective Hamiltonian are removed and we obtain the usual irreducible self-energy $\Sigma_{11'}(\omega)$ of the single-particle Dyson equation by putting an index “irreducible” on the $2p - 1h$ Green's function in eq. (10).

The same scenario remains valid if we take for A and B more complicated operators like e.g. the density operator $a_k^\dagger a_{k'}$. Again only the $(1p - 1h)$ irreducible parts of the $2p - 2h$ Green's function in eq. (10) contribute to the effective Hamiltonian.

A. Self-Consistent Random Phase Approximation

As discussed above, the effective Hamiltonian splits, also in the general case, in an instantaneous and an energy dependent part. The instantaneous part can be considered as a generalized Hartree-Fock Hamiltonian (see below). Therefore, as a first approximation, one can try to solve this “HF problem”, neglecting the resonant part of the effective Hamiltonian. As we will see later, this allows us to solve e.g. the two-body problem on the level of a Schrödinger-like equation for a single-frequency Green's function, in contrast to the Bethe-Salpeter case where a three-frequency Green's function has to be determined. This means that we can introduce two-particle states with shifted energies. Therefore, the consideration of the instantaneous part of the effective Hamiltonian can be understood as a direct generalization of the common single-particle HF approximation to the more-body or cluster case. In the past, this has been called *Cluster Mean Field* (CMF)⁵ or *Self-Consistent Random Phase Approximation* (SCRPA)^{4,9}. In the remainder of this paper, we will adopt SCRPA as shorthand for our approach, which, for the two-body case, can be connected to a variational principle (see appendix A).

In analogy to the single-particle Green's function we thus can define a generalized n -body mean-field propagator by substituting the instantaneous part of the effective Hamiltonian $\mathcal{H}_{AB}^{\text{SC}}$ back into the formal solution of the Dyson equation (8):

$$\begin{aligned} \langle\langle A; B \rangle\rangle_\omega^{\text{SC}} &= \left\{ \omega - \mathcal{H}_{AB}^{\text{SC}} \right\}^{-1} \mathcal{N} \\ &= \left\{ \omega - \langle [[A, H], B]_{-\epsilon} \rangle \mathcal{N}^{-1} \right\}^{-1} \mathcal{N} \end{aligned} \quad (14)$$

Usually it is possible, as we will illustrate in an example below, to close the system of equations in the following sense: For a full set of operators A and B and for a two-particle interaction *all* expectation values in $\mathcal{H}_{AB}^{\text{SC}}$ can be determined self-consistently from the Green's function (14) via the spectral theorem. For retarded Green's functions, the spectral theorem at temperature $\beta = 1/(k_B T)$ reads¹¹:

$$\langle AB \rangle^c \equiv \langle AB \rangle - \langle A \rangle \langle B \rangle$$

$$\begin{aligned}
&= -\frac{1}{\pi} \int_{-\infty}^{\infty} d\omega \frac{\text{Im} \langle\langle A; B \rangle\rangle_{\omega}^{\text{ret}}}{1 - \epsilon e^{-\beta\omega}} \\
&\xrightarrow{T \rightarrow 0} -\frac{1}{\pi} \int_0^{\infty} d\omega \text{Im} \langle\langle A; B \rangle\rangle_{\omega}^{\text{ret}} \\
\langle [A, B]_{-\epsilon} \rangle &= -\frac{1}{\pi} \int_{-\infty}^{\infty} d\omega \text{Im} \langle\langle A; B \rangle\rangle_{\omega}^{\text{ret}} .
\end{aligned} \tag{15}$$

The first of the eqs. (15) is the well-known *fluctuation-dissipation theorem*. The superscript ‘‘c’’ indicates that we calculate a correlated expectation value, i.e. fluctuations of $\langle AB \rangle$ around their classical mean value $\langle A \rangle \langle B \rangle$. This expectation value is known as *cumulant* or, in the sense of Feynman graphs, *connected* average¹². As indicated in eq. (15), the Fermi function in the spectral theorem for correlation functions $\langle AB \rangle^c$ reduces to a step function as $T \rightarrow 0$. The commutator expectation values, such as $\langle [A, B]_{-\epsilon} \rangle$, depend only implicitly on temperature, since the Green’s function occurring in the spectral theorem (15) is temperature dependent.

From now on, we will restrict ourselves to the $T = 0$ case, leaving the finite temperature consideration to forthcoming investigations.

B. Energy Weighted Sum Rule

The well-known energy weighted sum rule or f -sum rule connects the imaginary part of the exact Green’s function $\langle\langle A; B \rangle\rangle_{\omega}$ to the expectation value of the double commutator $\langle [[A, H], B]_{-\epsilon} \rangle$. Sometimes it is possible to choose operators A and B such that the double commutator $\langle [[A, H], B]_{-\epsilon} \rangle$ can be evaluated analytically. In this case, the sum rule may be used as a rigorous check for any approximative Green’s function.

Let us recall briefly the derivation of the sum rule. We can compute $\langle [[A, H], B]_{-\epsilon} \rangle$ using the spectral theorem (15) for the higher Green’s function $\langle\langle [A, H]; B \rangle\rangle_{\omega}$,

$$\langle [[A, H], B]_{-\epsilon} \rangle = -\frac{1}{\pi} \int_{-\infty}^{\infty} d\omega \text{Im} \langle\langle [A, H]; B \rangle\rangle_{\omega}^{\text{ret}} . \tag{16}$$

Inserting the equation of motion (4) on the rhs. and supposing the norm matrix to be real, we find the well-known energy weighted sum rule¹³:

$$\langle [[A, H], B]_{-\epsilon} \rangle = -\frac{1}{\pi} \int_{-\infty}^{\infty} d\omega \omega \text{Im} \langle\langle A; B \rangle\rangle_{\omega}^{\text{ret}} \tag{17}$$

We will now show that the sum rule (17) also holds for the SCRPA Green’s function $\langle\langle A; B \rangle\rangle_{\omega}^{\text{SC}}$. From eq. (14) we see that $\langle\langle A; B \rangle\rangle_{\omega}^{\text{SC}}$ satisfies the equation of motion

$$\omega \langle\langle A; B \rangle\rangle_{\omega}^{\text{SC}} = \mathcal{N} + \langle [[A, H], B]_{-\epsilon} \rangle \mathcal{N}^{-1} \langle\langle A; B \rangle\rangle_{\omega}^{\text{SC}} \tag{18}$$

rather than (4). Again, the norm matrix and the double commutator on the rhs. are real and ω independent. Inserting (18) into (17) and applying the spectral theorem (15) yields the norm matrix on the rhs. (which is cancelled by \mathcal{N}^{-1}).

From the above we see that, because of the double commutator structure of the effective Hamiltonian \mathcal{H}^{SC} , the SCRPA Green’s function fulfills the energy weighted sum rule (17) practically by construction.

C. Particle–hole propagator

As a concrete example, we will derive the SCRPA expression for a particle–hole Green’s function $\langle\langle a_p^+ a_k; a_{k'}^+ a_{p'} \rangle\rangle_{\omega}^{\text{ret}}$ in a fermionic system with general two–body interactions as described by the Hamiltonian (12). Since the operators defining the Green’s function are pairs of fermions, we will use the commutator Green’s function ($\epsilon = +1$).

For a homogeneous system, the kinetic energy is diagonal in momentum space,

$$t_{kk'} = \delta_{kk'} \varepsilon_k , \quad (19)$$

with k standing for momentum and other quantum numbers such as spin.

The norm matrix is also diagonal,

$$\begin{aligned} \mathcal{N}_{kpk'p'} &\equiv \left\langle [a_p^+ a_k, a_{k'}^+ a_{p'}]_- \right\rangle \\ &= \delta_{kk'} \delta_{pp'} (n_p - n_k) , \end{aligned} \quad (20)$$

where

$$n_k = \langle a_k^+ a_k \rangle \quad (21)$$

stands for the occupation numbers. The effective SCRPA Hamiltonian, introduced in eq. (11), can be worked out for the Hamiltonian (12). Using summation convention, this yields

$$\begin{aligned} \mathcal{H}_{kpk'p'}^{\text{SC}} &\equiv \left\langle [[a_p^+ a_k, H], a_{k'}^+ a_{p'}]_- \right\rangle (n_{p'} - n_{k'})^{-1} \\ &= \delta_{kk'} \delta_{pp'} (\varepsilon_k - \varepsilon_p) + (n_p - n_k) \bar{v}_{p'kk'p} \\ &\quad + \left[\frac{1}{2} \delta_{pp'} \bar{v}_{kq_2q_3q_4} \langle a_{k'}^+ a_{q_2}^+ a_{q_3} a_{q_4} \rangle^c + \frac{1}{2} \delta_{kk'} \bar{v}_{q_1q_2q_3p} \langle a_{q_1}^+ a_{q_2}^+ a_{q_3} a_{p'} \rangle^c \right. \\ &\quad + \frac{1}{2} \bar{v}_{p'kq_3q_4} \langle a_{k'}^+ a_p^+ a_{q_3} a_{q_4} \rangle^c + \frac{1}{2} \bar{v}_{q_1q_2pk'} \langle a_{q_1}^+ a_{q_2}^+ a_k a_{p'} \rangle^c \\ &\quad \left. - \bar{v}_{kq_2q_3k'} \langle a_p^+ a_{q_2}^+ a_{q_3} a_{p'} \rangle^c - \bar{v}_{p'q_2q_3p} \langle a_{k'}^+ a_{q_2}^+ a_{q_3} a_k \rangle^c \right] (n_{p'} - n_{k'})^{-1} , \end{aligned} \quad (22)$$

where ε_k denote the Hartree–Fock corrected single–particle energies,

$$\varepsilon_k = \varepsilon_k + \bar{v}_{kqkq} n_q . \quad (23)$$

As we will see in section IID, the second term in eq. (22), $(n_p - n_k) \bar{v}_{p'kk'p}$, will lead us to a RPA–like theory. We will use the term RPA in a slightly broader sense than usual and already account for the exchange term of the interaction, see eq. (23). The term in brackets, in contrast, contains exclusively correlated expectation values (i.e. cumulant averages¹²),

$$\langle a_{q_1}^+ a_{q_2}^+ a_{q_3} a_{q_4} \rangle^c \equiv \langle a_{q_1}^+ a_{q_2}^+ a_{q_3} a_{q_4} \rangle - [\langle a_{q_1}^+ a_{q_4} \rangle \langle a_{q_2}^+ a_{q_3} \rangle - \langle a_{q_1}^+ a_{q_3} \rangle \langle a_{q_2}^+ a_{q_4} \rangle] \quad (24)$$

not taken into account by usual RPA–like theories.

The SCRPA Green’s function

$$\mathcal{G}_{kpk'p'}^{\text{SC}}(\omega) = \langle\langle a_p^+ a_k; a_{k'}^+ a_{p'} \rangle\rangle_{\omega}^{\text{SC}} \quad (25)$$

defined in eq. (14), can now be obtained by inverting the matrix $[\omega - \mathcal{H}_{kpk'p'}^{\text{SC}}]$. Once it is determined, all elements of the effective Hamiltonian (22) and the norm matrix (20) can be calculated via the spectral theorem (15). Moreover, it is possible to derive an explicit expression for the occupation numbers n_p by summing the diagonal elements of the norm matrix, $n_p - n_k$, over the index k .

With the commutator spectral theorem (15) and the k –space volume

$$\mathcal{V} = \sum_k 1 , \quad (26)$$

we get for the occupation numbers

$$n_p = \frac{1}{\mathcal{V}} \sum_k n_k - \frac{1}{\pi \mathcal{V}} \sum_k \int_{-\infty}^{\infty} d\omega \text{Im} \langle\langle a_p^+ a_k; a_k^+ a_p \rangle\rangle_{\omega}^{\text{ret}} . \quad (27)$$

In a continuous system, it is necessary to introduce a cutoff in order to keep the k -space volume \mathcal{V} finite. In lattice systems, as will be seen in section III, \mathcal{V} is finite, since the k -sum is restricted to the first Brillouin zone.

The correlation functions $\langle a_{q_1}^+ a_{q_2}^+ a_{q_3} a_{q_4} \rangle^c$ in eq. (22) are connected to those, which are accessible via the spectral theorem (15),

$$\langle (a_{q_1}^+ a_{q_4}) \cdot (a_{q_2}^+ a_{q_3}) \rangle^c \equiv \langle a_{q_1}^+ a_{q_4} a_{q_2}^+ a_{q_3} \rangle - \langle a_{q_1}^+ a_{q_4} \rangle \langle a_{q_2}^+ a_{q_3} \rangle . \quad (28)$$

This yields

$$\langle a_{q_1}^+ a_{q_2}^+ a_{q_3} a_{q_4} \rangle^c = -\frac{1}{\pi} \int_0^\infty d\omega \operatorname{Im} \langle\langle a_{q_1}^+ a_{q_4}; a_{q_2}^+ a_{q_3} \rangle\rangle_\omega^{\text{ret}} - \langle a_{q_1}^+ a_{q_3} \rangle [\delta_{q_2 q_4} - \langle a_{q_2}^+ a_{q_4} \rangle] , \quad (29)$$

where for a homogeneous system the last term on the rhs. is related to the occupation numbers by momentum conservation.

The system of equations is now closed and can be iterated to self-consistency. We therefore start with an assumption for the expectation values in \mathcal{H}^{SC} and \mathcal{N} . The SCRPA Green's function, obtained by matrix inversion, then allows us to calculate new values for the elements of the effective Hamiltonian and the norm matrix by applying the spectral eqs. (27) and (29). The new \mathcal{H}^{SC} and \mathcal{N} lead us to the next approximation for the Green's function and so forth.

D. RPA and Self-Consistent RPA

We now analyze the contributions to the SCRPA Green's function by rewriting eq. (7) as an integral equation:

$$\mathcal{G}_{kp'p'}^{\text{SC}}(\omega) = \mathcal{G}_{kp'p'}^0(\omega) + \sum_{\substack{k_1 p_1 \\ k_2 p_2}} \mathcal{G}_{kp'k_1 p_1}^0(\omega) \mathcal{K}_{k_1 p_1 k_2 p_2}^{\text{SC}} \mathcal{G}_{k_2 p_2 k' p'}^{\text{SC}}(\omega) , \quad (30)$$

where $\mathcal{G}_{kp'p'}^0(\omega)$ has the structure of a free particle-hole Green's function,

$$\mathcal{G}_{kp'p'}^0(\omega) = \delta_{kk'} \delta_{pp'} \frac{n_p - n_k}{\omega - (\epsilon_k - \epsilon_p) + i0^+} . \quad (31)$$

The integral kernel $\mathcal{K}_{k_1 p_1 k_2 p_2}^{\text{SC}}$ represents the interaction occurring in the effective Hamiltonian (22),

$$\mathcal{K}_{kp'p'}^{\text{SC}} = (n_p - n_k)^{-1} [\mathcal{H}_{kp'p'}^{\text{SC}} - \delta_{kk'} \delta_{pp'} (\epsilon_k - \epsilon_p)] . \quad (32)$$

Since the kernel \mathcal{K}^{SC} splits up into a RPA-like part

$$\mathcal{K}_{kp'p'}^{\text{RPA}} \equiv \bar{v}_{p'kk'p} \quad (33)$$

and a remainder, \mathcal{K}^c , which only contains correlated two-body densities, it is convenient to rewrite eq. (30) in a different way (using matrix notation)

$$\mathcal{G}^{\text{SC}} = \mathcal{G}^{\text{RPA}} + \mathcal{G}^{\text{RPA}} \mathcal{K}^c \mathcal{G}^{\text{SC}} \quad (34)$$

$$\mathcal{G}^{\text{RPA}} = \mathcal{G}^0 + \mathcal{G}^0 \mathcal{K}^{\text{RPA}} \mathcal{G}^{\text{RPA}} \quad (35)$$

At this point, we emphasize that the eq. (35) has exactly the same structure as the usual RPA equation. However, in our theory the occupation numbers can and will, even at zero temperature, be different from the Hartree-Fock values

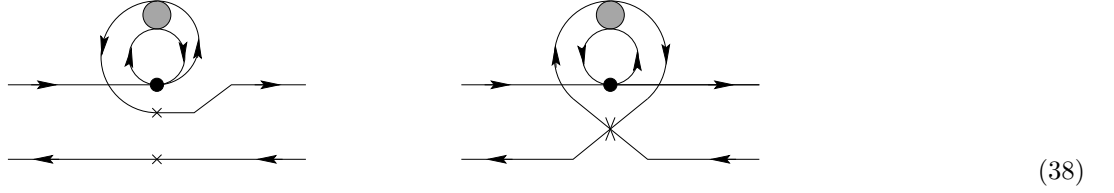
$$n_k^{\text{HF}} = \Theta(E_F - \epsilon_k) . \quad (36)$$

In the following, we will consider the eq. (35) as generic for the RPA whatever the occupation numbers will be. We will label it *pure RPA* if the occupation numbers are fixed to their HF values (36). In contrast, a theory in which the occupation numbers are determined self-consistently from the RPA Green's function or contain correlations in any other way will be called *renormalized RPA*².

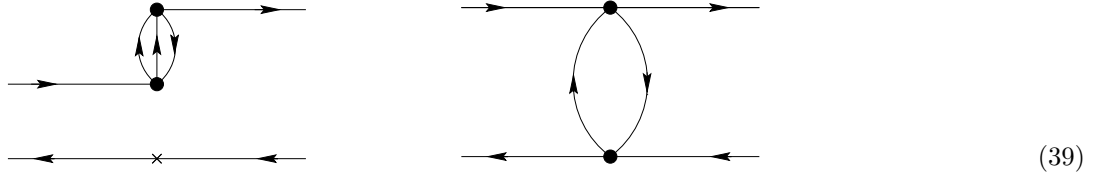
In SCRPA, eq. (34) is coupled to the RPA eq. (35), upgrading the (renormalized) RPA to the Self-Consistent RPA. Comparing eq. (30) to eq. (35) clearly shows that the RPA structure of the solution is preserved when passing over to self-consistent RPA:

$$\begin{aligned}\mathcal{G}^{\text{SC}}(\omega) &= [1 - \mathcal{G}^0(\omega) \mathcal{K}^{\text{SC}}]^{-1} \mathcal{G}^0(\omega) \\ \mathcal{G}^{\text{RPA}}(\omega) &= [1 - \mathcal{G}^0(\omega) \mathcal{K}^{\text{RPA}}]^{-1} \mathcal{G}^0(\omega)\end{aligned}\quad (37)$$

The improvement contained in the integral kernel \mathcal{K}^c can be interpreted by the following connected diagrams:

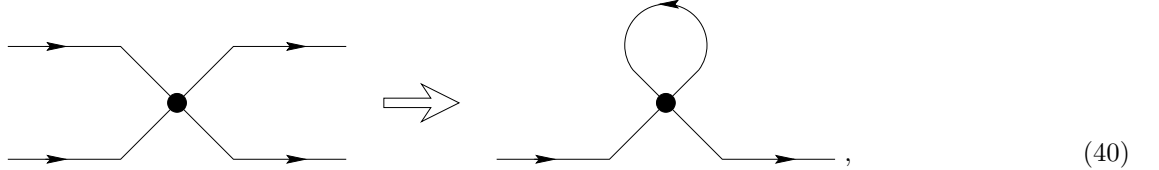


The hatched circle represents a correlated particle–hole propagator and the dot stands for the antisymmetrized interaction \bar{v} . The crosses represent Kronecker symbols in momentum and other quantum numbers, and δ –functions in time. We see that the first graph in eq. (38) corresponds to a coupling of the single–particle motion to the density fluctuations, i.e. a self–energy correction, whereas the second graph describes an induced (screened) interaction. Of course analogous graphs exist where the interaction is attached to the hole line. Again, we want to emphasize that *all* terms in eq. (38) are instantaneous. We obtain the second–order contributions in replacing the hatched circle in eq. (38) by an interaction dot:

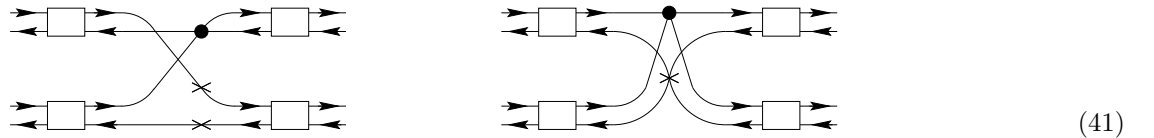


Cutting the graphs in eq. (39) between the two interactions occurring one an infinitesimal time after the other illustrates the instantaneous coupling of the $1p1h$ and $2p2h$ spaces. Solving the eqs. (35) and (34) self-consistently thus constitutes a partial resummation of the interaction to a very high order.

Just as the Hartree–Fock self–energy for a single particle can be constructed from a two–particle interaction term by attaching an outgoing to an incoming line, viz.



we may interpret eq. (38) as the Hartree–Fock field for density–density fluctuations (this point of view has actually been adopted in ref.⁵). In analogy, we can reconstruct the loops in eq. (38) by closing two density fluctuation lines in the following first–order terms for the interaction (which can be obtained from perturbation theory):



Considering all exchange terms it is possible to reconstruct exactly the effective Hamiltonian (22) which therefore represents the mean–field Hamiltonian of a gas of quantal fluctuations present in any many fermion system.

III. APPLICATION TO THE HUBBARD MODEL

In this section, we will apply the SCRPA, developed in section II, to density–density correlation functions in the Hubbard model.

The single–band Hubbard Hamiltonian describes electrons hopping on a lattice with an on–site interaction U ¹⁴:

$$H = \sum_{ij\sigma} t_{ij} a_{i\sigma}^+ a_{j\sigma} + U \sum_i \hat{n}_{i\uparrow} \hat{n}_{i\downarrow} \quad (42)$$

where $a_{i\sigma}^+$ and $a_{i\sigma}$ denote the creation and destruction operators for an electron with spin σ on site i , respectively. The occupation number operator on site i is defined as $\hat{n}_{i\sigma} = a_{i\sigma}^+ a_{i\sigma}$. In the following, we will restrict ourselves to nearest neighbour hopping

$$t_{ij} = -t (\delta_{j,i+1} + \delta_{j,i-1}) , \quad (43)$$

repulsive interactions $U > 0$, and zero temperature. We will work with $\hbar = 1$, set the lattice spacing to unity ($a = 1$) and measure energies in units of the hopping integral ($t = 1$).

After Fourier transformation, the Hamiltonian reads

$$H = \sum_{\mathbf{k}\sigma} \varepsilon_{\mathbf{k}} a_{\mathbf{k}\sigma}^+ a_{\mathbf{k}\sigma} + \frac{U}{N} \sum_{\mathbf{k}\mathbf{p}\mathbf{q}} a_{\mathbf{k}\uparrow}^+ a_{\mathbf{k}+\mathbf{q}\uparrow} a_{\mathbf{p}\downarrow}^+ a_{\mathbf{p}-\mathbf{q}\downarrow} . \quad (44)$$

Notice that N is the number of sites (ions, not electrons) and all momentum sums run over the first Brillouin zone unless indicated differently. The single-particle dispersion relation in the hyper-cubic lattice is given by the Fourier transform of the nearest neighbour hopping matrix element (43),

$$\varepsilon_{\mathbf{k}} = -2 \sum_{i=1}^d \cos k_i , \quad (45)$$

where d denotes the dimension.

A. Charge- and longitudinal spin-density correlations

In the following, we will examine the behaviour of charge- and spin-density fluctuations in the Hubbard model. Therefore, we will introduce the density operator

$$\rho_{\mathbf{q}\sigma} = \sum_{\mathbf{k}} a_{\mathbf{k}\sigma}^+ a_{\mathbf{k}+\mathbf{q}\sigma} , \quad (46)$$

which is the Fourier transform of the Wannier number operator $\hat{n}_{i\sigma}$. It will be used to describe charge and longitudinal spin fluctuations. Summing over the spins gives rise to the charge susceptibility

$$\chi^{\text{ch}}(\mathbf{q}, \omega) = \frac{1}{N} \left\langle\left\langle (\rho_{\mathbf{q}\uparrow} + \rho_{\mathbf{q}\downarrow}); (\rho_{\mathbf{q}\uparrow}^+ + \rho_{\mathbf{q}\downarrow}^+) \right\r\rangle_{\omega}^{\text{ret}} . \quad (47)$$

As from now on we will use only retarded Green's functions, we will omit the superscript "ret" on correlation functions.

The z -component of the spin on site i can be expressed as the difference between the number of \uparrow -spins and \downarrow -spins on that site, or, after Fourier transformation,

$$S_{\mathbf{q}}^z = \frac{1}{2} (\rho_{\mathbf{q}\uparrow} - \rho_{\mathbf{q}\downarrow}) . \quad (48)$$

Correlations between the z -components of the spins are described by the longitudinal spin susceptibility,

$$\begin{aligned} \chi^{\text{sp}}(\mathbf{q}, \omega) &= \frac{1}{N} \left\langle\left\langle S_{\mathbf{q}}^z; S_{\mathbf{q}}^{z+} \right\r\rangle_{\omega} \right. \\ &= \frac{1}{N} \left\langle\left\langle \frac{1}{2} (\rho_{\mathbf{q}\uparrow} - \rho_{\mathbf{q}\downarrow}); \frac{1}{2} (\rho_{\mathbf{q}\uparrow}^+ - \rho_{\mathbf{q}\downarrow}^+) \right\r\rangle_{\omega} . \end{aligned} \quad (49)$$

We will now examine the charge and longitudinal spin susceptibilities, $\chi^{\text{ch}}(\mathbf{q}, \omega)$ and $\chi^{\text{sp}}(\mathbf{q}, \omega)$ in SCRPA. Therefore, we introduce the particle-hole Green's function

$$\mathcal{G}_{\mathbf{k}\sigma\mathbf{p}\sigma'}(\mathbf{q}, \omega) \equiv \left\langle\left\langle a_{\mathbf{k}\sigma}^+ a_{\mathbf{k}+\mathbf{q}\sigma}; a_{\mathbf{p}+\mathbf{q}\sigma'}^+ a_{\mathbf{p}\sigma'} \right\r\rangle_{\omega} . \quad (50)$$

In contrast to the general particle-hole propagator defined in section II C, we will now account for momentum conservation right from the beginning. As the derivation of the SCRPA propagator is completely analogous to section II C, we will only state the results.

The norm matrix (20) is given by

$$\mathcal{N}_{\mathbf{k}\sigma\mathbf{p}\sigma'}(\mathbf{q}) = \delta_{\mathbf{k}\mathbf{p}}\delta_{\sigma\sigma'} (n_{\mathbf{k}\sigma} - n_{\mathbf{k}+\mathbf{q}\sigma}) , \quad (51)$$

where $n_{\mathbf{k}\sigma}$ denotes the occupation number for the Bloch state \mathbf{k} with spin σ defined in analogy to eq. (21). The effective Hamiltonian, which was defined for a general two-body interaction in eq. (22), reads for the Hubbard Hamiltonian

$$\begin{aligned} \mathcal{H}_{\mathbf{k}\sigma\mathbf{p}\sigma'}^{\text{SC}}(\mathbf{q}) &= \delta_{\mathbf{k}\mathbf{p}}\delta_{\sigma\sigma'} [\varepsilon_{\mathbf{k}+\mathbf{q}} - \varepsilon_{\mathbf{k}}] + \delta_{\sigma,-\sigma'} (n_{\mathbf{k}\sigma} - n_{\mathbf{k}+\mathbf{q}\sigma}) \frac{U}{N} \\ &+ \left[-\delta_{\mathbf{k}\mathbf{p}}\delta_{\sigma\sigma'} \frac{U}{N} \sum_{\mathbf{q}'} \left\langle \left(a_{\mathbf{k}+\mathbf{q}-\mathbf{q}'\sigma}^+ a_{\mathbf{k}\sigma} + a_{\mathbf{k}+\mathbf{q}\sigma}^+ a_{\mathbf{k}+\mathbf{q}'\sigma} \right) \rho_{\mathbf{q}-\mathbf{q}',-\sigma} \right\rangle^c \right. \\ &\quad + \delta_{\sigma\sigma'} \frac{U}{N} \left\langle a_{\mathbf{k}\sigma}^+ a_{\mathbf{p}\sigma} \rho_{\mathbf{k}-\mathbf{p},-\sigma} + a_{\mathbf{p}+\mathbf{q}\sigma}^+ a_{\mathbf{k}+\mathbf{q}\sigma} \rho_{\mathbf{p}-\mathbf{k},-\sigma} \right\rangle^c \\ &\quad + \delta_{\sigma,-\sigma'} \frac{U}{N} \sum_{\mathbf{q}'} \left\langle \left(a_{\mathbf{k}\sigma}^+ a_{\mathbf{k}+\mathbf{q}-\mathbf{q}'\sigma} - a_{\mathbf{k}+\mathbf{q}'\sigma}^+ a_{\mathbf{k}+\mathbf{q}\sigma} \right) \right. \\ &\quad \left. \left. \cdot \left(a_{\mathbf{p}+\mathbf{q}-\mathbf{q}',-\sigma}^+ a_{\mathbf{p},-\sigma} - a_{\mathbf{p}+\mathbf{q},-\sigma}^+ a_{\mathbf{p}+\mathbf{q}',-\sigma} \right) \right\rangle^c \right] \cdot (n_{\mathbf{p}\sigma'} - n_{\mathbf{p}+\mathbf{q}\sigma'})^{-1} , \quad (52) \end{aligned}$$

with $\rho_{\mathbf{q}\sigma}$ being the density operator introduced in eq. (46). The Hartree-Fock corrections to the single-particle energies cancel because of the on-site (and thus momentum independent) interaction.

The spectral theorem yields for the occupation numbers (see eq. (27))

$$n_{\mathbf{k}\sigma} = \langle n_{\sigma} \rangle - \frac{1}{\pi N} \sum_{\mathbf{q}} \int_{-\infty}^{\infty} d\omega \text{Im} \mathcal{G}_{\mathbf{k}\sigma\mathbf{k}\sigma}(\mathbf{q}, \omega) , \quad (53)$$

where $\langle n_{\sigma} \rangle$ denotes the number of σ -electrons per site. In the paramagnetic phase, spin-broken expectation values like $\langle a_{\mathbf{k}\uparrow}^+ a_{\mathbf{k}\downarrow} \rangle$ vanish, and we obtain from equation (29) for the correlation functions occurring in the effective Hamiltonian (52):

$$\left\langle a_{\mathbf{k}\uparrow}^+ a_{\mathbf{k}+\mathbf{q}\uparrow} a_{\mathbf{p}+\mathbf{q}\downarrow}^+ a_{\mathbf{p}\downarrow} \right\rangle^c = -\frac{1}{\pi} \int_0^{\infty} d\omega \text{Im} \mathcal{G}_{\uparrow\mathbf{p}\downarrow}(\mathbf{q}, \omega) \quad (54)$$

As in section II C, the system of equations is now closed and can be iterated to self-consistency, since, on one hand, we are able to calculate all elements of the effective Hamiltonian $\mathcal{H}_{\mathbf{k}\sigma\mathbf{p}\sigma'}^{\text{SC}}(\mathbf{q})$ from the particle-hole propagator, and, on the other hand, the latter by a matrix inversion for every \mathbf{q} and ω :

$$\mathcal{G}_{\mathbf{k}\sigma\mathbf{p}\sigma'}^{\text{SC}}(\mathbf{q}, \omega) = [\omega - \mathcal{H}_{\mathbf{k}\sigma\mathbf{p}\sigma'}^{\text{SC}}(\mathbf{q})]^{-1} (n_{\mathbf{p}\sigma'} - n_{\mathbf{p}+\mathbf{q}\sigma'}) \quad (55)$$

We will see in section III C that the corresponding system of equations for spin-density correlations is not closed onto itself, but couples back to the charge-density correlations.

As shown in section II C (see eqs. (34,35)), it is advised to first calculate the RPA particle-hole propagator before solving the full SCRPA problem (55). For the Hubbard interaction, the RPA kernel \mathcal{K}^{RPA} defined in eq. (33) is nothing but the interaction per site

$$\mathcal{K}_{\mathbf{k}\sigma\mathbf{p}\sigma'}^{\text{RPA}}(\mathbf{q}) = \delta_{\sigma,-\sigma'} \frac{U}{N} . \quad (56)$$

Eq. (35) can therefore be written as an integral equation coupling $\mathcal{G}_{\mathbf{k}\sigma\mathbf{p}\sigma'}^{\text{RPA}}(\mathbf{q}, \omega)$ and $\mathcal{G}_{\mathbf{k}-\sigma\mathbf{p}\sigma'}^{\text{RPA}}(\mathbf{q}, \omega)$:

$$\mathcal{G}_{\mathbf{k}\sigma\mathbf{p}\sigma'}^{\text{RPA}}(\mathbf{q}, \omega) = \delta_{\mathbf{k}\mathbf{p}}\delta_{\sigma\sigma'} \mathcal{G}_{\mathbf{k}\sigma}^0(\mathbf{q}, \omega) + \mathcal{G}_{\mathbf{k}\sigma}^0(\mathbf{q}, \omega) \frac{U}{N} \sum_{\mathbf{k}'} \mathcal{G}_{\mathbf{k}'-\sigma\mathbf{p}\sigma'}^{\text{RPA}}(\mathbf{q}, \omega) , \quad (57)$$

where $\mathcal{G}_{\mathbf{k}\sigma}^0(\mathbf{q}, \omega)$ defines the renormalized free particle-hole propagator

$$\mathcal{G}_{\mathbf{k}\sigma}^0(\mathbf{q}, \omega) = \frac{(n_{\mathbf{k}\sigma} - n_{\mathbf{k}+\mathbf{q}\sigma})}{\omega - [\varepsilon_{\mathbf{k}+\mathbf{q}} - \varepsilon_{\mathbf{k}}] + i0^+} . \quad (58)$$

In terms of Feynman graphs, this means substituting the SCRPA kernel $\mathcal{K}_{\mathbf{k}\sigma\mathbf{p}\sigma'}^{\text{SC}}(\mathbf{q})$ in the integral eq. (30) by its RPA expression, which is nothing but a spin-flip interaction, represented by a dot,

The diagram shows the RPA kernel $\mathcal{K}_{\mathbf{k}\sigma\mathbf{p}\sigma'}^{\text{RPA}}(\mathbf{q})$ as a sum of two terms. The first term is a direct interaction represented by a shaded rectangle with incoming lines (\mathbf{k}, σ) and $(\mathbf{k} + \mathbf{q}, \sigma)$ and outgoing lines (\mathbf{p}, σ') and $(\mathbf{p} + \mathbf{q}, \sigma')$. The second term is a spin-flip interaction represented by a dot with a U label, where the incoming lines (\mathbf{k}, σ) and $(\mathbf{k} + \mathbf{q}, \sigma)$ meet at the dot, and the outgoing lines (\mathbf{p}, σ') and $(\mathbf{p} + \mathbf{q}, \sigma')$ meet at another dot, with a shaded rectangle between them. The spin labels $-\sigma$ are shown on the lines between the dots.

The physical interpretation of eq. (57) is that in RPA the Hubbard interaction flips the spin of the electron on each and every scattering process. This is certainly a good approximation for an electron propagating in an antiferromagnetically ordered state. In this case, we see from Fig. 1 that a \downarrow -electron added to the \uparrow -electron on site i cannot hop off because all their neighbours have spin \downarrow , too. Therefore it must be the \uparrow -electron which hops to a neighbouring site. Arriving there, it can only hop the same way back to its original site. Otherwise, the \uparrow -electron is surrounded by other \uparrow -electrons and thus frozen in. As this process continues, an extra electron propagating in an antiferromagnet from site i to site j flips every spin on its trajectory. Thus, neglecting higher-order loop trajectories, the electron's path is completely retraceable. This case was first examined by Brinkman and Rice¹⁵ who showed that this “retraceable path approximation” is accurate for walks up to length twelve for the analogous case of an extra hole propagating in an antiferromagnetic spin configuration. Moreover, they showed that even if the spins are randomly distributed rather than antiferromagnetically ordered, the dominant contribution to the hole Green's function comes from retraceable paths.

In this line of reasoning, the dimensionality of the system plays a crucial role. In one dimension, antiferromagnetic long-range order is forbidden by the Mermin–Wagner theorem¹⁶. Nevertheless, as there are no loop trajectories in one dimension, the retraceable path approximation becomes exact for any spin configuration.

In dimensions $d \geq 3$, antiferromagnetic ordering is possible. As the number of nearest neighbors increases, loop trajectories become less probable. Therefore, the retraceable path approximation gets exact to order $\mathcal{O}(1/d^4)$ ¹⁷.

Moreover, in higher dimensions the correlations are weaker than in lower ones. As we derived the RPA kernel $\mathcal{K}_{\mathbf{k}\sigma\mathbf{p}\sigma'}^{\text{RPA}}(\mathbf{q})$ by neglecting the correlations present in the SCRPA, we expect it to be more accurate in higher dimensions than in lower ones. We will see in section IV that, even in one dimension, the renormalized RPA solution shows a Mott–Hubbard transition at a finite critical interaction strength, which, for half filling is of the order of the bandwidth. This scenario, which can be considered as generic for the RPA, is certainly wrong for the one dimensional case. Nevertheless, in higher dimensions it could be quite realistic. There, this viewpoint is also supported by methods like e.g. the Hubbard-III approximation^{18,19}.

Iterating the integral eq. (57), we can decouple the equations for $\mathcal{G}_{\mathbf{k}\sigma\mathbf{p}\sigma}^{\text{RPA}}(\mathbf{q}, \omega)$ and $\mathcal{G}_{\mathbf{k}\sigma\mathbf{p}-\sigma}^{\text{RPA}}(\mathbf{q}, \omega)$,

$$\begin{aligned} \mathcal{G}_{\mathbf{k}\sigma\mathbf{p}\sigma}^{\text{RPA}}(\mathbf{q}, \omega) &= \delta_{\mathbf{k}\mathbf{p}} \mathcal{G}_{\mathbf{k}\sigma}^0(\mathbf{q}, \omega) + \mathcal{G}_{\mathbf{k}\sigma}^0(\mathbf{q}, \omega) U \chi_{-\sigma}^0(\mathbf{q}, \omega) \frac{U}{N} \sum_{\mathbf{k}'} \mathcal{G}_{\mathbf{k}'\sigma\mathbf{p}\sigma}^{\text{RPA}}(\mathbf{q}, \omega) \\ \mathcal{G}_{\mathbf{k}\sigma\mathbf{p}-\sigma}^{\text{RPA}}(\mathbf{q}, \omega) &= \mathcal{G}_{\mathbf{k}\sigma}^0(\mathbf{q}, \omega) \frac{U}{N} \mathcal{G}_{\mathbf{p}-\sigma}^0(\mathbf{q}, \omega) + \mathcal{G}_{\mathbf{k}\sigma}^0(\mathbf{q}, \omega) U \chi_{-\sigma}^0(\mathbf{q}, \omega) \frac{U}{N} \sum_{\mathbf{k}'} \mathcal{G}_{\mathbf{k}'\sigma\mathbf{p}-\sigma}^{\text{RPA}}(\mathbf{q}, \omega), \end{aligned} \quad (60)$$

where we introduced the renormalized non-interacting susceptibility

$$\chi_{\sigma}^0(\mathbf{q}, \omega) = \frac{1}{N} \sum_{\mathbf{k}} \mathcal{G}_{\mathbf{k}\sigma}^0(\mathbf{q}, \omega). \quad (61)$$

Eq. (60) can be solved explicitly for the particle–hole Green's function, yielding

$$\begin{aligned} \mathcal{G}_{\mathbf{k}\sigma\mathbf{p}\sigma}^{\text{RPA}}(\mathbf{q}, \omega) &= \mathcal{G}_{\mathbf{k}\sigma}^0(\mathbf{q}, \omega) \left[\delta_{\mathbf{k}\mathbf{p}} + \frac{U}{N} \mathcal{G}_{\mathbf{p}\sigma}^0(\mathbf{q}, \omega) \frac{U \chi_{-\sigma}^0(\mathbf{q}, \omega)}{1 - U \chi_{\uparrow}^0(\mathbf{q}, \omega) U \chi_{\downarrow}^0(\mathbf{q}, \omega)} \right] \quad \text{and} \\ \mathcal{G}_{\mathbf{k}\sigma\mathbf{p}-\sigma}^{\text{RPA}}(\mathbf{q}, \omega) &= \mathcal{G}_{\mathbf{k}\sigma}^0(\mathbf{q}, \omega) \frac{U}{N} \mathcal{G}_{\mathbf{p}-\sigma}^0(\mathbf{q}, \omega) \frac{1}{1 - U \chi_{\uparrow}^0(\mathbf{q}, \omega) U \chi_{\downarrow}^0(\mathbf{q}, \omega)}. \end{aligned} \quad (62)$$

Finally, we have to determine the occupation numbers $n_{\mathbf{k}\sigma}$ self-consistently from the RPA Green's function (62). As will be explained in more detail in section IV A, this is a somewhat delicate procedure. Indeed, initiating the iteration cycle, at small U , with the Fermi step for $n_{\mathbf{k}\sigma}$, one inevitably picks up some spin instabilities when summing over \mathbf{q} in eq. (53). These instabilities correspond to poles in the RPA Green's function at purely imaginary frequencies. This entails that we may create some unphysical values when applying the spectral theorem to such a Green's function. For example, integrating $\text{Im} \mathcal{G}_{\mathbf{k}\sigma\mathbf{p}-\sigma}^{\text{RPA}}(\mathbf{q}, \omega)$ over the whole ω -axis yields an unphysical finite value if the Green's function

has poles at imaginary frequencies. As this integral is connected via the spectral theorem (15) to a commutator, we know that it has to be zero. When iterating the system of non-linear equations, it turns out that this pathology is cured. The occupation numbers get rounded thus weakening the interaction in such a way that finally the imaginary spin poles disappear. At self-consistency, the integral of $\text{Im} \mathcal{G}_{\mathbf{k}\sigma \mathbf{p}-\sigma}^{\text{RPA}}(\mathbf{q}, \omega)$ over all frequencies vanishes for every \mathbf{q} , as it is expected from the spectral theorem.

For completeness, we state that *fixing* the occupation to their Hartree–Fock values brings us from *renormalized* back to *pure* RPA:

$$n_{\mathbf{k}\sigma}^{\text{HF}} = \Theta(E_{\text{F}} - \varepsilon_{\mathbf{k}}) \quad (63)$$

In section III B, an energy weighted sum rule is shown to be fulfilled in both, renormalized and Self-Consistent RPA. In pure RPA it is only fulfilled as long as all eigenfrequencies are real. As will be pointed out in section IV F, this is closely connected to the problem of RPA instabilities.

If we restrict ourselves to the paramagnetic phase, we have $n_{\mathbf{k}\uparrow} = n_{\mathbf{k}\downarrow}$ implying $\chi_{\uparrow}^0(\mathbf{q}, \omega) = \chi_{\downarrow}^0(\mathbf{q}, \omega)$. We can thus recover the usual RPA structure for the susceptibilities $\chi^{\text{ch}}(\mathbf{q}, \omega)$ and $\chi^{\text{sp}}(\mathbf{q}, \omega)$ by combining the two equations (62) and summing over \mathbf{k} and \mathbf{p} :

$$\begin{aligned} \chi^{\text{ch}}(\mathbf{q}, \omega) &= \frac{1}{N} \sum_{\mathbf{k}\mathbf{p}\sigma} [\mathcal{G}_{\mathbf{k}\sigma \mathbf{p}\sigma}^{\text{RPA}}(\mathbf{q}, \omega) + \mathcal{G}_{\mathbf{k}\sigma \mathbf{p}-\sigma}^{\text{RPA}}(\mathbf{q}, \omega)] \\ &= \frac{2\chi^0(\mathbf{q}, \omega)}{1 - U\chi^0(\mathbf{q}, \omega)} \\ \chi^{\text{sp}}(\mathbf{q}, \omega) &= \frac{1}{4N} \sum_{\mathbf{k}\mathbf{p}\sigma} [\mathcal{G}_{\mathbf{k}\sigma \mathbf{p}\sigma}^{\text{RPA}}(\mathbf{q}, \omega) - \mathcal{G}_{\mathbf{k}\sigma \mathbf{p}-\sigma}^{\text{RPA}}(\mathbf{q}, \omega)] \\ &= \frac{\frac{1}{2}\chi^0(\mathbf{q}, \omega)}{1 + U\chi^0(\mathbf{q}, \omega)} \end{aligned} \quad (64)$$

B. Energy weighted sum rule

The fact that the density operators $\rho_{\mathbf{q}\sigma}$ commute with the interaction term of the Hubbard Hamiltonian (44) gives us the possibility to evaluate $\left\langle \left[[\rho_{\mathbf{q}\sigma}, H], \rho_{\mathbf{q}\sigma'}^+ \right]_- \right\rangle$ analytically. In analogy to section II B, we thus can establish an energy weighted sum rule for the exact susceptibilities $\chi^{\text{ch}}(\mathbf{q}, \omega)$ and $\chi^{\text{sp}}(\mathbf{q}, \omega)$. We will now discuss the fulfillment of the sum rule for the SCRPA, the renormalized RPA, and the pure RPA Green's functions.

In the first place, we calculate the double commutator

$$\begin{aligned} \left\langle \left[[\rho_{\mathbf{q}\sigma}, H], \rho_{\mathbf{q}\sigma'}^+ \right]_- \right\rangle &= \delta_{\sigma\sigma'} \sum_{\mathbf{k}} [\varepsilon_{\mathbf{k}+\mathbf{q}} - \varepsilon_{\mathbf{k}}] (n_{\mathbf{k}\sigma} - n_{\mathbf{k}+\mathbf{q}\sigma}) \\ &= \delta_{\sigma\sigma'} 2 \sum_{i=1}^d (\cos q_i - 1) \sum_{k_i} \varepsilon_{\{k_i\}} n_{\{k_i\}\sigma} \end{aligned} \quad (65)$$

where k_i are the components of the vector \mathbf{k} . The only contributions to the double commutator come from the kinetic term of the Hamiltonian (44), since, as mentioned above, $\rho_{\mathbf{q}\sigma}$ commutes with the interaction. Remark that for a $\mathbf{k}^2/(2m)$ dispersion law the rhs. of (65) yields the well-known result $\langle n_{\sigma} \rangle \mathbf{q}^2/m$ (see ref.¹³).

As pointed out in section II B for the general case, the expectation value of the double commutator (65) is related to the imaginary part of the exact retarded susceptibility by an energy weighted integral (see eq. (17)):

$$\left\langle \left[[\rho_{\mathbf{q}\sigma}, H], \rho_{\mathbf{q}\sigma'}^+ \right] \right\rangle = -\frac{1}{\pi} \int_{-\infty}^{\infty} d\omega \omega \text{Im} \left\langle \left\langle \rho_{\mathbf{q}\sigma}; \rho_{\mathbf{q}\sigma'}^+ \right\rangle_{\omega}^{\text{ret}} \right\rangle \quad (66)$$

The SCRPA Green's function was shown to satisfy the sum rule (66) as well, since the double commutator on the lhs. can be expressed by the SCRPA Hamiltonian (52) and the norm matrix (51):

$$\begin{aligned}
\left\langle \left[[\rho_{\mathbf{q}\sigma}, H], \rho_{\mathbf{q}\sigma'}^+ \right] \right\rangle &= \sum_{\mathbf{k}\mathbf{p}} \sum_{\mathbf{p}_1\sigma_1} \mathcal{H}_{\mathbf{k}\sigma \mathbf{p}_1\sigma_1}^{\text{SC}}(\mathbf{q}) \mathcal{N}_{\mathbf{p}_1\sigma_1 \mathbf{p}\sigma'}(\mathbf{q}) \\
&= \sum_{\mathbf{k}\mathbf{p}} \mathcal{H}_{\mathbf{k}\sigma \mathbf{p}\sigma'}^{\text{SC}}(\mathbf{q}) (n_{\mathbf{p}\sigma'} - n_{\mathbf{p}+\mathbf{q}\sigma'})
\end{aligned} \tag{67}$$

In the view of our formalism this may seem evident. However, theories which generalize the RPA approach do not necessarily fulfill the f -sum rule. Above all, we notice that in eq. (67) *all* terms containing correlations from the effective Hamiltonian $\mathcal{H}_{\mathbf{k}\sigma \mathbf{p}\sigma'}^{\text{SC}}(\mathbf{q})$ cancel when summing over \mathbf{k} and \mathbf{p} . In *renormalized* RPA, on the other hand, we neglect these correlations right from the beginning (see eqs. (56,57)). Consequently, the renormalized RPA susceptibilities fulfill the energy weighted sum rule (66), too. Moreover, it is well-known^{10,20} that the *pure* RPA susceptibilities satisfy the sum rule (66) if the expectation value on the lhs. is evaluated with the Hartree–Fock ground state wave function. However, this statement only holds true as long as all RPA frequencies are real.

Finally, we find the energy weighted sum rules for $\chi^{\text{ch}}(\mathbf{q}, \omega)$ and $\chi^{\text{sp}}(\mathbf{q}, \omega)$ by combining eq. (66) for the different spin configurations according to the definitions of the charge susceptibility (47) and longitudinal spin susceptibility (49), respectively:

$$\begin{aligned}
2 \sum_{i=1}^d (\cos q_i - 1) \langle \hat{t}^i \rangle &= -\frac{1}{\pi} \int_{-\infty}^{\infty} d\omega \omega \text{Im} \chi^{\text{ch}}(\mathbf{q}, \omega) \\
\frac{1}{2} \sum_{i=1}^d (\cos q_i - 1) \langle \hat{t}^i \rangle &= -\frac{1}{\pi} \int_{-\infty}^{\infty} d\omega \omega \text{Im} \chi^{\text{sp}}(\mathbf{q}, \omega)
\end{aligned} \tag{68}$$

On the lhs., we introduced the shorthand

$$\langle \hat{t}^i \rangle = \frac{1}{N} \sum_{k_i\sigma} \varepsilon_{\{k_i\}} n_{\{k_i\}\sigma}, \tag{69}$$

standing for the contribution to the mean kinetic energy per site provided by the electron motion in i direction. It should be stressed that $\langle \hat{t}^i \rangle$ depends on the occupation numbers $n_{\mathbf{k}\sigma}$ and thus implicitly on the Green's function. In contrast, for the usual $\mathbf{k}^2/(2m)$ dispersion law, the double commutator in eq. (65) depends on the mean number of electrons per site (i.e. the filling) instead of $\langle \hat{t}^i \rangle$, and is therefore a model independent quantity. In our case of a cosine dispersion law, however, the \mathbf{q} -dependence of the sum rule provides a check which does not depend on the Green's function or any other assumption.

C. Transverse spin–density correlations

In this section, for completeness, we will shortly discuss the transverse spin response. The spin–flip operators S_i^\pm may be substituted in the usual way by combination of an annihilation operator of a σ electron and a creation operator of a $-\sigma$ electron. After Fourier transformation to momentum space, we obtain

$$S_{\mathbf{q}}^+ = \sum_{\mathbf{k}} a_{\mathbf{k}\uparrow}^+ a_{\mathbf{k}+\mathbf{q}\downarrow} \quad \text{and} \quad S_{\mathbf{q}}^- = \sum_{\mathbf{k}} a_{\mathbf{k}+\mathbf{q}\downarrow}^+ a_{\mathbf{q}\uparrow}. \tag{70}$$

Correlations between the spin–flip operators give rise to the transverse spin susceptibility

$$\chi^{+-}(\mathbf{q}, \omega) = \frac{1}{N} \langle\langle S_{\mathbf{q}}^+; S_{\mathbf{q}}^- \rangle\rangle_{\omega}. \tag{71}$$

In order to examine the transverse spin susceptibility in SCRPA, we introduce the following correlation functions:

$$\mathcal{G}_{\mathbf{k}\sigma \mathbf{p}\sigma'}^{\text{trans}}(\mathbf{q}, \omega) \equiv \langle\langle a_{\mathbf{k}\sigma}^+ a_{\mathbf{k}+\mathbf{q},-\sigma}; a_{\mathbf{p}+\mathbf{q},-\sigma'}^+ a_{\mathbf{p}\sigma'} \rangle\rangle_{\omega} \tag{72}$$

In complete analogy to the charge–density case (see section III A), we calculate the norm matrix by evaluating the commutator of the two operators defining the Green's function (see eq. (20)):

$$\mathcal{N}_{\mathbf{k}\sigma \mathbf{p}\sigma'}^{\text{trans}}(\mathbf{q}) = \delta_{\mathbf{k}\mathbf{p}} \delta_{\sigma\sigma'} (n_{\mathbf{k}\sigma} - n_{\mathbf{k}+\mathbf{q},-\sigma}) \tag{73}$$

The effective SCRPA Hamiltonian reads in analogy to eq. (22)

$$\begin{aligned}
\mathcal{H}_{\mathbf{k}\sigma\mathbf{p}\sigma'}^{\text{trans}}(\mathbf{q}) &= \delta_{\mathbf{k}\mathbf{p}}\delta_{\sigma\sigma'} [\epsilon_{\mathbf{k}+\mathbf{q},-\sigma} - \epsilon_{\mathbf{k}\sigma}] - \delta_{\sigma\sigma'} (n_{\mathbf{k}\sigma} - n_{\mathbf{k}+\mathbf{q},-\sigma}) \frac{U}{N} \\
&+ \left[-\delta_{\mathbf{k}\mathbf{p}}\delta_{\sigma\sigma'} \frac{U}{N} \sum_{\mathbf{q}'} \left\langle a_{\mathbf{k}+\mathbf{q},-\sigma}^+ a_{\mathbf{k}+\mathbf{q}',-\sigma} a_{\mathbf{q}-\mathbf{q}'\sigma} \rho_{\mathbf{q}-\mathbf{q}'\sigma} + a_{\mathbf{k}+\mathbf{q}-\mathbf{q}'\sigma}^+ a_{\mathbf{k}\sigma} \rho_{\mathbf{q}-\mathbf{q}',-\sigma} \right\rangle^c \right. \\
&\quad - \delta_{\sigma\sigma'} \frac{U}{N} \sum_{\mathbf{q}'} \left\langle \left(a_{\mathbf{k}\sigma}^+ a_{\mathbf{k}+\mathbf{q}-\mathbf{q}'\sigma} - a_{\mathbf{k}+\mathbf{q}',-\sigma}^+ a_{\mathbf{k}+\mathbf{q},-\sigma} \right) \cdot \left(a_{\mathbf{p}+\mathbf{q}-\mathbf{q}'\sigma}^+ a_{\mathbf{p}\sigma} - a_{\mathbf{p}+\mathbf{q},-\sigma}^+ a_{\mathbf{p}+\mathbf{q}',-\sigma} \right) \right\rangle^c \\
&\quad \left. - \delta_{\sigma,-\sigma'} \frac{U}{N} \left\langle a_{\mathbf{k}\sigma}^+ a_{\mathbf{p},-\sigma} S_{\mathbf{k}-\mathbf{p}}^\sigma + a_{\mathbf{p}+\mathbf{q}\sigma}^+ a_{\mathbf{k}+\mathbf{q},-\sigma} S_{\mathbf{p}-\mathbf{k}}^\sigma \right\rangle^c \right] \cdot (n_{\mathbf{p}\sigma'} - n_{\mathbf{p}+\mathbf{q},-\sigma'})^{-1}, \quad (74)
\end{aligned}$$

with $\rho_{\mathbf{q}\sigma}$ denoting the density operator introduced in eq. (46) and $S_{\mathbf{q}}^\sigma$ being a spin-flip operator defined in analogy to $S_{\mathbf{q}}^+$ (see eq. (70)):

$$S_{\mathbf{q}}^\sigma = \sum_{\mathbf{k}} a_{\mathbf{k}\sigma}^+ a_{\mathbf{k}+\mathbf{q},-\sigma} \quad (75)$$

The Hartree-Fock corrected single-particle energies defined in eq. (23) are given by

$$\epsilon_{\mathbf{k}\sigma} = \varepsilon_{\mathbf{k}} + U \langle n_{-\sigma} \rangle. \quad (76)$$

In contrast to the charge-density case, not *all* elements of the effective Hamiltonian (74) can be determined self-consistently from the Green's functions (72). The calculation of terms like $\left\langle a_{\mathbf{k}\uparrow}^+ a_{\mathbf{k}+\mathbf{q}-\mathbf{q}'\uparrow} a_{\mathbf{p}+\mathbf{q}-\mathbf{q}'\uparrow}^+ a_{\mathbf{p}\uparrow} \right\rangle^c$, for example, cannot be performed with the spectral theorem for spin-flip Green's functions, since they contain always the same number of \uparrow and \downarrow spins. These terms can, however, be determined from the charge-density Green's function introduced section III A. By this means, the transverse spin susceptibility is coupled to the charge-density susceptibilities χ^{ch} and χ^{sp} . In this work, however, we will not further investigate the transverse spin excitations.

IV. RESULTS FOR THE CHARGE AND THE LONGITUDINAL SPIN RESPONSE IN THE HUBBARD CHAIN

As a first application of our general formalism, we will calculate the charge and longitudinal spin correlation functions $\chi^{\text{ch}}(q, \omega)$ and $\chi^{\text{sp}}(q, \omega)$ in the one-dimensional Hubbard model. This will also serve as a test of whether our formalism is well behaved in a numerical sense.

It was explained in section III A that the first step will consist in calculating the Green's function $\mathcal{G}_{k\sigma p\sigma'}(q, \omega)$, introduced in eq. (50), on the level of the *renormalized* RPA. In this paper, we will not go beyond this approximation. Indeed, the numerical solution of the full SCRPA problem turns out to be quite enormous and certainly needs a major numerical effort which is intended to be invested in future work. Nevertheless, the main characteristics of the self-consistency cycle are already present on the level of the renormalized RPA.

We thus will determine self-consistently the RPA Green's function (62) together with the occupation numbers $n_{k\sigma}$. Due to the self-consistency, the occupation numbers are "renormalized" which modifies the Green's function $\mathcal{G}_{k\sigma}^0(q, \omega)$ and the susceptibility $\chi^0(q, \omega)$ occurring in the RPA propagator (62).

In contrast, in pure RPA, i.e. if we fix the occupation numbers to their Hartree-Fock values given by eq (63), $\mathcal{G}_{k\sigma}^0(q, \omega)$ and $\chi^0(q, \omega)$ are identical with the free particle-hole propagator and susceptibility, respectively.

After a brief overview of the numerical method we will discuss the results for the renormalized RPA in the infinite Hubbard chain in the paramagnetic phase, i.e. $n_{k\uparrow} = n_{k\downarrow}$.

A. Numerical Method

In order to determine the renormalized RPA Green's function, we have to solve the RPA eqs. (58,61,62) consistently with the equation for the occupation numbers, (53).

Therefore, we start with an assumption for the initial occupation numbers and set up the following iteration cycle:

- Set up the renormalized free Green's function (58) from the current set of occupation numbers.

- Calculate the renormalized free susceptibility (61) by integrating $\mathcal{G}_{k\sigma}^0(q, \omega)$ over k . Note that for the computation of $\text{Im}\chi^0(q, \omega)$ it is convenient to introduce a small but finite imaginary part “ $i0^+$ ” in the denominator of $\mathcal{G}_{k\sigma}^0(q, \omega)$.
- Set up the RPA Green’s function (62) from $\mathcal{G}_{k\sigma}^0(q, \omega)$ and $\chi^0(q, \omega)$.
- Compute a new set of occupation numbers by performing the spectral integral in eq. (53). This task is also simplified by assuming a finite “ $i0^+$ ”.
- Repeat the iteration cycle from the beginning until self-consistency is achieved.

Usually, we will start with a small interaction, e.g. $U = 1$, and a Fermi step for the occupation numbers. For this U , the RPA equations are then iterated to self-consistency. The result is used to initialize the occupation numbers of an iteration cycle with a slightly higher interaction. We thus increase the interaction in small steps, iterating each time to self-consistency, until the desired value for U is reached. This procedure has the advantage that the spin response, in contrast to pure RPA, remains stable throughout the whole calculation.

The momentum integrations are performed by summing over a grid of uniformly distributed points in the first Brillouin zone. The number of points is typically 256.

Energy integrals are computed using a grid of points obeying a Lorentzian distribution peaked at $\omega = 0$. The number of energy points is typically 2048 and the half width half maximum of the distribution is about twice the bandwidth, i.e. 8.

As mentioned above, it is convenient for computational purposes to introduce a small but finite imaginary part “ $i0^+$ ” in the denominator of the renormalized free Green’s function $\mathcal{G}_{k\sigma}^0(q, \omega)$. Typically we use values of the order of magnitude of $i/16$ which corresponds to $1/64$ the bandwidth. It can be shown that within our resolution the results are not affected by slight variations of this value.

B. Occupation numbers

Fig.2 shows the momentum distribution function

$$n_k = \frac{1}{2} (n_{k\uparrow} + n_{k\downarrow}) \quad (77)$$

of the half-filled Hubbard chain. The renormalized RPA results are compared with Quantum Monte-Carlo calculations. We see that, for small U , the renormalized RPA momentum distribution has a discontinuity at the Fermi edge. This is typical for Fermi liquids, and thus indicates a metallic behaviour. For large U , the renormalized RPA momentum distribution is continuous, and our theory predicts an insulating ground state. Increasing U in small steps ($1/4$), we deduce that within our numerical momentum resolution the discontinuity at k_F vanishes at $U \approx 3$. We thus find a Mott metal-insulator transition at an interaction strength which is slightly smaller than the band width (i.e. 4). This is in good agreement with approximations designed for the Hubbard model in higher dimensions, like e.g. the Hubbard-III solutions^{18,19}. In *one dimension*, however, the exact solution⁸ predicts an insulating ground state for any finite U . Consequently, the exact results for n_k , known from Quantum Monte-Carlo (QMC)²¹ for finite U and from Bethe ansatz in the limit of large U ^{22,23}, show a smooth behaviour over the whole k range for all interactions.

This disagreement should be judged in the light that the effective Hamiltonian of the renormalized RPA neglects *all* correlation functions. As discussed in section III A, this approximation is expected to be far better in higher dimensions. Nevertheless, in the strong coupling limit, our theory reproduces the cosine-behaviour for n_k , known from the Bethe ansatz expansion, apart from the prefactor (see section IV G).

Away from half filling, the renormalized RPA predicts a similar scenario: For small U , the momentum distribution function shows a discontinuity at k_F , which now persists up to higher interaction strengths as in the half filled case. For the quarter filled chain, e.g., this jump lasts up to $U \approx 4$, as can be seen from Fig. 3. The discontinuity occurs precisely at the same $k = k_F$ as the step in the momentum distribution of the free Fermi gas. Therefore, the renormalized RPA satisfies the Luttinger theorem in one dimension²⁴.

Again, the Mott-Hubbard transition predicted by our theory is in disagreement with the exact behaviour away from half filling, which is known to be a Luttinger liquid for all interaction strengths. The latter is characterized by a power law singularity in the momentum distribution at the Fermi points, which is expected in the strong coupling limit from both, Bethe ansatz expansions²⁵⁻²⁷ and QMC calculations²¹. For finite interaction strengths, it was also detected by QMC studies of infinite Hubbard chains²⁸.

Calculations of finite chains indicate a discontinuity at k_F decreasing only very slowly with increasing chain length N ^{29,30}. Therefore, they have great difficulties to detect the Luttinger liquid behaviour. There are certain similarities

between finite chains and calculations using a finite number of points in the Brillouin zone as e.g. the numerical solution of the renormalized RPA equations. Nevertheless, our calculations indicate a finite slope of the momentum distribution on both sides of the Fermi points, and we do not find any signature of Luttinger liquid behaviour.

C. Renormalized free susceptibility $\chi^0(q, \omega)$

1. Imaginary part

Before discussing the RPA response functions $\chi^{\text{ch}}(q, \omega)$ and $\chi^{\text{sp}}(q, \omega)$ let us analyze the renormalization effects in the free susceptibility $\chi^0(q, \omega)$.

In the (q, ω) -plane, the imaginary part of $\chi^0(q, \omega)$ is restricted to the region, where particle-hole excitations exist, i.e. there must be a k for which $\omega = \varepsilon_{k+q} - \varepsilon_k$ is satisfied, or,

$$|\omega| \leq \left| 4 \sin \frac{q}{2} \right| . \quad (78)$$

If the occupation numbers are step functions like in the free Fermi gas, a second boundary condition is provided by the fact, that in the particle-hole continuum described by eq. (78) there must be at least one k -vector for which the numerator of the free Green's function (58), $(n_{k\sigma} - n_{k+q\sigma})$, does not vanish. This yields

$$|\omega| \geq 2 |\cos(k_F) - \cos(k_F - |q|)| . \quad (79)$$

We have seen in section III A that the Hartree-Fock corrections to the single-particle energies cancel. Hence, the denominator of the free Green's function (58) does not change throughout the renormalization process, and eq. (78) represents a rigid boundary for the imaginary part of the free susceptibility. On the other hand, any rounding of the occupation numbers will directly affect the second boundary condition, (79). This behaviour of the imaginary part is illustrated in Fig. 4 for half filling and $q = \pi/2$. We see that $\text{Im} \chi^{\text{free}}(q, \omega)$, represented by the dotted line, is only nonzero in the domain in between the two boundaries given by eq. (78) and eq. (79).

In section IV A, we explained that for technical reasons we have to set “ $i0^+$ ” in the denominator of $\mathcal{G}_{k\sigma}^0(q, \omega)$ to a small but finite value in order to perform the integral in eq. (61). This smoothens the numerically calculated free susceptibility (dot-dashed line) in comparison to the analytical expression given in appendix B (dotted line).

Let us now study the imaginary part of the renormalized free susceptibility, $\text{Im} \chi^0(q, \omega)$, represented by the continuous line in Fig. 4 for half filling, $U = 3$ and $q = \pi/2$. On the outer boundary (78) it behaves essentially in the same way as $\text{Im} \chi^{\text{free}}(q, \omega)$, whereas the inner boundary (79) is completely washed out due to the renormalization of the occupation numbers $n_{k\sigma}$.

As will be discussed in section IV G, the strong coupling limit of our theory can be calculated analytically for half filling. Scaling our strong coupling result for $\text{Im} \chi^0(q, \omega)$ down to $U = 3$ leads to the dashed line in Fig. 4. For $U = 3$, which is lower than the bandwidth and has thus to be considered as an intermediate interaction, $\text{Im} \chi^0$ of the complete renormalized RPA calculation (continuous line) qualitatively already resembles the properly scaled strong coupling result (dashed line).

Fig. 5 shows $\text{Im} \chi^0(q, \omega)$ for $U = 6$ and half filling. Comparing the continuous with the dashed line, we notice that the renormalized RPA result for $\text{Im} \chi^0$ now agrees also quantitatively very well with the corresponding strong coupling result. The remaining difference comes from the finite imaginary part “ $i0^+$ ” used for the numerical computation of $\text{Im} \chi^0(q, \omega)$.

2. Real part

Let us now examine the real part of the free susceptibility $\chi^{\text{free}}(q, \omega)$. As can be seen from the analytic expressions given in appendix B, $\text{Re} \chi^{\text{free}}(q, \omega)$ diverges at the two boundaries of $\text{Im} \chi^{\text{free}}(q, \omega)$ which demark the particle-hole continuum.

The divergence on the upper boundary, given by eq. (78), makes the denominator of the pure RPA charge susceptibility (see eq. (64)), $1 - U\chi^{\text{free}}(q, \omega)$, vanish at an energy above the continuum limit where an undamped plasmon is created.

This is illustrated in Fig. 6 by the intersection of the horizontal line at $+1/U$ with the real part of $\chi^{\text{free}}(q, \omega)$ at $\omega \approx 3.3$. The dotted and dot-dashed lines represent the analytical or numerical expressions for $\text{Re} \chi^{\text{free}}(q, \omega)$, respectively. Hence, as U is increased, the horizontal line at $1/U$ is lowered and the pure RPA plasmon is shifted towards higher energies.

A similar scenario can be established for the longitudinal spin response in the pure RPA. Its denominator, $1 + U\chi^{\text{free}}(q, \omega)$, vanishes at an energy below the lower continuum limit, given by eq. (79), and an undamped magnon is created. Again, this is shown in Fig. 6 by the intersection of the horizontal line at $-1/U$ with $\text{Re}\chi^{\text{free}}$ at $\omega \approx 1.6$. As the interaction is increased, the magnon is shifted towards lower frequencies, and as it reaches $\omega = 0$, the system becomes unstable. This will be discussed in more detail below. Note that slightly below the upper continuum edge, the dotted line representing $\text{Re}\chi^{\text{free}}$ also meets the horizontal line at $-1/U$. However, as $\text{Im}\chi^{\text{free}}$ is large in this region near the square-root singularity at the upper continuum boundary, it will not contribute to the pure RPA spin response.

Fig. 7 and Fig. 8 display the position of the plasmons and the magnons in the (q, ω) -plane for $U = 3$ and for half and quarter filling, respectively. Once more, we notice that the pure RPA plasmons lie above the particle-hole continuum, represented by the dotted area. The pure RPA magnons occur below the lower continuum boundary. As the lower boundary goes to $\omega = 0$ for $q \rightarrow 2k_F$, the spin pole will meet the momentum axis near $2k_F$ producing the well-known Peierls instability. This instability occurs in the pure RPA for infinitesimal U exactly at $q = 2k_F$. When increasing the interaction, the region of instability is enlarged covering a growing interval around $q = 2k_F$.

It extends to the whole q -axis when U exceeds some critical interaction U^{Stoner} , provided by Stoner's mean-field theory³¹. In mean field, the paramagnetic state, $m = \langle n_{\uparrow} \rangle - \langle n_{\downarrow} \rangle = 0$, is always a local extremum in the energy surface as a function of the magnetization m . This extremum is a minimum for

$$U < U^{\text{Stoner}} = 2\pi \sin \frac{\pi n}{2}, \quad (80)$$

with n denoting the number of electrons per site. For $U > U^{\text{Stoner}}$ it is a maximum. Nevertheless, it should be remembered that there is a range of interactions $U^{\text{MF}} < U < U^{\text{Stoner}}$ for which the paramagnetic state is a local but not the global minimum, and that the global minimum is reached in the fully ferromagnetic state $n = m$.

We thus conclude that the pure RPA only produces valid results in the region where no instabilities occur. Calculating quantities having a contribution from the unstable region around $q = 2k_F$, like e.g. the occupation numbers, does not make sense even for small interactions. Above U^{Stoner} , the pure RPA is unstable for all q and ω . As we will see below, it is the virtue of the renormalized RPA (and also the SCRPA) to cure these instabilities, rendering possible the computation of the occupation numbers from eq. (53). These arguments will be underlined in section IV F by considering the energy weighted sum rule.

Above the outer continuum limit (78), the real part of the renormalized free susceptibility, $\text{Re}\chi^0(q, \omega)$, behaves qualitatively like $\text{Re}\chi^{\text{free}}(q, \omega)$. In the same manner as above, we find an undamped plasmon at the energy where the denominator of the renormalized charge susceptibility in eq. (64), $1 - U\chi^0(q, \omega)$, vanishes. For small U , the plasmon is only slightly shifted to lower energies with respect to the pure RPA plasmon. For larger U , the renormalization effects are stronger. We will see in section IV G that the frequencies of the renormalized plasmons remain finite as U goes to infinity. The pure RPA plasmons, in contrast, occur at infinite frequencies in the limit of large U .

Below the outer continuum limit (78), the renormalization effects in $\text{Re}\chi^0(q, \omega)$ are more drastic. This is shown by the continuous line in Fig. 6 for $U = 3$ and half filling. The singularity of $\text{Re}\chi^{\text{free}}$ at the lower continuum boundary ($\omega \approx 2$) is completely damped and $\text{Re}\chi^0$ is an almost structure-less function within the renormalized continuum, i.e. from $\omega = 0$ up to almost the continuum edge (78) at $\omega \approx 2.8$.

This gives, even for small interactions, rise to qualitative changes in the longitudinal spin response. At the energy where the denominator of the longitudinal spin susceptibility, $1 + U\chi^0(q, \omega)$, becomes resonant, the imaginary part of $\chi^0(q, \omega)$ is large. Therefore, the renormalized spin response will show a broad maximum instead of the undamped magnon found in the pure RPA spin response.

Apart from the qualitative differences expected between the pure and the renormalized RPA spin responses, there are important consequences for the regime where the pure RPA is unstable. We recall that in this q -range, the pure RPA magnon frequency becomes imaginary and the magnon pole in the pure RPA spin response disappears. As one consequence, we will outline in section IV F that the energy weighted sum rule for the pure RPA spin response will be violated.

In contrast, the broad maximum in the renormalized RPA spin response will persist even for the q -vectors where the pure RPA is unstable. Therefore, the renormalized RPA spin response fulfills the energy weighted sum rule for every q , even for interactions $U > U^{\text{Stoner}}$. This will be explained in more detail in section IV F. By this means, the Peierls instability occurring in the pure RPA is cured by the renormalization process.

In the limit of large interactions, the real part of χ^0 becomes completely flat within the renormalized particle-hole continuum, and $1 + U\text{Re}\chi^0(q, \omega)$ vanishes within the *whole* continuum. As $\text{Im}\chi^0(q, \omega)$ is smallest within the continuum for $\omega \rightarrow 0$, the broad maximum in the longitudinal spin response is shifted towards zero frequency. The consequences are discussed in chapter IV E.

We finally remark that even for small U , the renormalization effects are strong enough to lock $\text{Re}\chi^0(q, \omega)$ to values greater or equal $-1/U$ (see Fig. 6). Consequently, the scenario given above is valid, and the renormalized spin response

shows already for weak interaction strengths a broad continuum peak rather than a sharp magnon pole.

D. Charge response

Due to the rather small renormalization effects of $\chi^0(q, \omega)$ outside the particle–hole continuum, we expect the charge response in the pure and in the renormalized RPA to behave similarly.

For intermediate interactions, the pure RPA charge response is given by a rather small continuum which is limited by the two boundary conditions (78) and (79), and an undamped plasmon lying above the continuum. This is illustrated for $U = 3$ and half filling by the dotted line in Fig. 9, where we used the analytical expressions for χ^{free} , given in appendix B, to evaluate the pure RPA charge response. Evaluating the pure RPA charge response numerically, i.e. with a finite value of “ $i0^+$ ” as discussed in section IV A, leads to the dot–dashed line in Fig. 9. We observe that, due to the finite “ $i0^+$ ”, the pure RPA plasmon at $\omega \approx 3.3$ is broadened with respect to the analytical curve, and that the sharp cutoff at the continuum boundaries is smoothed.

Comparing the continuous line with the dot–dashed line in Fig. 9 shows that the renormalized charge response agrees essentially with the pure RPA predictions. As explained in section IV C 2, the main differences are that the tail of the renormalized charge continuum now goes down to $\omega = 0$ and that the plasmon is slightly shifted towards lower energies. The precise position of the renormalized plasmon is indicated in Fig. 9 by a continuous vertical line in the center of the numerically computed plasmon pole which, for numerical reasons, has a finite width.

Qualitatively, the charge response for $U = 3$ is already very similar to the properly scaled strong coupling limit of our theory. This can be seen by comparing the dashed and the continuous lines in Fig. 9. Moreover, the plasmon position of the pure RPA and the strong coupling limit of the renormalized RPA agree very well, such that the dotted and the dashed vertical lines cannot be resolved from another. Note, however, that this agreement is purely accidental.

The renormalization effects become more drastic as the interaction strength is increased. For half filling and $U = 6$ Fig. 10 illustrates that the renormalized charge continuum now not only goes down to $\omega = 0$ (continuous line) but also is much stronger than the pure RPA charge continuum (dot–dashed line). Further, the energy shift of the plasmon obtained from renormalization is larger than in the weak coupling limit.

For $U = 6$, the charge response already agrees quantitatively very well with the strong coupling limit of our theory. Comparing the continuous and the dashed line shows that both, the continuum contributions and the positions of the plasmon peaks are in good agreement. In section IV G we will discuss in detail that the renormalization prevents the plasmon pole in the large U limit from being shifted to infinite frequencies as this happens for the pure RPA plasmon.

Similar results are obtained away from half filling.

E. Longitudinal spin response

According to the discussion of the real parts of $\chi^{\text{free}}(q, \omega)$ and $\chi^0(q, \omega)$ in section IV C 2, we expect the spin response to change qualitatively when passing from pure to renormalized RPA, even in the regime of weak and intermediate coupling.

This is illustrated in Fig. 11 for $q = \pi/2$, $U = 3$ and half filling. For these values there are already significant changes, although the pure RPA is still stable. The pure RPA spin response (dot–dashed line) consists of a rather small continuum being restricted to the area in between the two boundaries given by eqs. (78) and (79), and an undamped magnon occurring below this continuum.

As explained before, the broadening of the magnon is of numerical origin. The corresponding analytic expression can be obtained using the representation of χ^{free} from appendix B. The latter leads to the dotted line in Fig. 11.

It was argued in section IV C 2 that the magnon pole disappears during the renormalization procedure. Hence, the renormalized RPA spin response is fully described by a continuum exhibiting a broad peak (continuous line). Like the renormalized charge continuum, this spin continuum starts at $\omega = 0$ and goes up to the upper continuum boundary (78). The dashed line in Fig. 11 shows the spin response in the strong coupling limit of our theory scaled to $U = 3$. A comparison with the renormalized RPA result (continuous line) shows that especially for low frequencies there are still important differences. Thus, at $U = 3$ the strong coupling limit is not yet reached.

If U is increased or if the q -vector is chosen in the domain around $2k_F$ where the pure RPA is unstable, the pure RPA magnon frequency will become purely imaginary. Fig. 12 shows this case for $U = 6$, $q = \pi/2$ and half filling. The pure RPA spin response is represented by the dot–dashed and the underlying dotted line, depending on whether the numerical or the analytical expression is monitored. We notice that the magnon peak in the pure RPA spin response vanishes completely. This corresponds to an unphysical situation, as will be underlined in section IV F by sum rule arguments.

In renormalized RPA, the broad maximum in the longitudinal spin response is shifted towards zero frequency when the interaction is increased. This can be seen by comparing the continuous lines in Fig. 11 and Fig. 12, which represent the renormalized spin response for $U = 3$ and $U = 6$, respectively. Whereas in Fig. 11, the renormalized spin response reaches its maximum at a finite frequency, we see from Fig. 12 that for $U = 6$ it is strongly peaked at $\omega = 0$. This behaviour is characteristic for the strong coupling limit of our theory, given by the dashed line which cannot be resolved from the continuous line in the latter graph. In renormalized RPA, the energy weighted sum rule is fulfilled for all U , as will be demonstrated in the next subsection. Nevertheless, we will point out in section IV G that the singularity of the spin response at $\omega = 0$ may lead to divergences in correlation functions.

F. Energy weighted sum rule

In section III B a sum rule is derived for the energy weighted spin and charge response. In the one-dimensional Hubbard model, eq. (68) connects an energy weighted integral over the response functions to the mean kinetic energy per site, $\langle \hat{t} \rangle$, times a form factor:

$$\begin{aligned} S_1^{\text{ch}}(q) : -2 \langle \hat{t} \rangle (1 - \cos q) &= -\frac{1}{\pi} \int_{-\infty}^{\infty} d\omega \omega \text{Im} \chi^{\text{ch}}(q, \omega) \\ S_1^{\text{sp}}(q) : -\frac{1}{2} \langle \hat{t} \rangle (1 - \cos q) &= -\frac{1}{\pi} \int_{-\infty}^{\infty} d\omega \omega \text{Im} \chi^{\text{sp}}(q, \omega) . \end{aligned} \quad (81)$$

In section III B it is argued that it not only holds true for the exact response functions $\chi^{\text{ch}}(q, \omega)$ and $\chi^{\text{sp}}(q, \omega)$ but as well for the response functions in Self-Consistent and in renormalized RPA if the mean kinetic energy per site, $\langle \hat{t} \rangle$, is calculated self-consistently from the corresponding Green's function.

Moreover, it is well known that the sum rule for the pure RPA response functions is fulfilled if $\langle \hat{t} \rangle$ is calculated with the Hartree-Fock ground-state *as long as no instability occurs*^{10,20}.

In Fig. 13, 14, 15 and 16 we show the result of the sum rule checks for $U = 3$, and for half and quarter filling, respectively. In all figures, the left hand sides of the eqs. (81) are plotted with the dotted lines. As their $(1 - \cos q)$ -behaviour is independent of the approximations made in the Green's function, we will consider them as "reference lines". Nevertheless, they are scaled with a prefactor, $\langle \hat{t} \rangle$, which depends on the Green's function. In renormalized RPA, the mean kinetic energy per site is less negative than in Hartree-Fock, since the momentum distribution is smoothened. Thus, the reference lines for the renormalized RPA sum rules lie always below the pure RPA lines.

For the *renormalized* RPA susceptibilities, the right hand sides of the eqs. (81) are represented by the continuous lines. They cannot be resolved from the corresponding dotted reference lines. Hence, in renormalized RPA the sum rule is fulfilled for all q -vectors and for both, the charge and the longitudinal spin response.

Calculating the rhs. of the eqs. (81) with the *pure* RPA susceptibilities yields the dashed lines. The sum rule for the charge response is monitored in the figures 13 and 15. There, the dashed lines cannot be resolved from their dotted reference lines. This means, that the sum rule for the pure RPA charge response holds true for all q -vectors.

In the figures 14 and 16, we show the sum rule check for the pure RPA spin response. The dashed lines, which represent the energy weighted pure RPA spin response, agree with their reference lines, apart from a range of q -vectors around the Peierls vector $2k_F$. This q -range coincides with the q -range where the corresponding magnon dispersion in Fig. 7 and Fig. 8, respectively, goes to $\omega = 0$. Therefore, the energy weighted sum rule for the pure RPA spin susceptibility is only fulfilled for the range of momenta where the pure RPA is stable.

Again, we want to emphasize the quality of the renormalized and the Self-Consistent RPA to restore the f -sum rule for *all* momenta and interactions.

G. The large U limit

At half filling and for large U , the occupation numbers predicted by renormalized RPA can be fitted very accurately by

$$n_{k\sigma} = \frac{1}{2} \left(1 + \frac{4}{U} \cos k \right) , \quad (82)$$

whereas the large U expansion of the Bethe ansatz solution yields^{22,23}

$$n_{k\sigma} = \frac{1}{2} \left(1 + \frac{8 \ln 2}{U} \cos k \right). \quad (83)$$

Comparing the dotted line and the lowest continuous line in Fig. 2 shows that for $U = 5$, the expression (82) agrees already very well with the numerical results for n_k . We will show in the following that eq. (82) indeed is the fully self-consistent solution of the renormalized RPA equations in the strong coupling limit.

Based on eq. (82), it is possible to give an explicit expression for the renormalized free susceptibility. As the continuum boundary condition for step-like occupation numbers, eq. (79), becomes meaningless in the limit of strong interactions, the only characteristic energy is provided by the upper continuum limit (78). Hence, the explicit expressions for $\chi^0(q, \omega)$ do not depend on q and ω as independent variables anymore, but can be denoted as a function of one single variable ξ , which is the energy in units of the upper continuum limit (78):

$$\xi = \frac{\omega}{|4 \sin \frac{q}{2}|} \quad (84)$$

Performing the integration in eq. (61) with occupation numbers as given by eq. (82) yields the renormalized free susceptibility

$$\chi^0(\xi) = -\frac{1}{U} \begin{cases} 1 + i \frac{\xi}{\sqrt{1-\xi^2}} & \text{for } |\xi| < 1 \\ 1 - \frac{|\xi|}{\sqrt{\xi^2-1}} & \text{for } |\xi| > 1 \end{cases}. \quad (85)$$

Like for the free susceptibility χ^{free} , the imaginary part of χ^0 still has a square root singularity at the continuum limit $|\xi| = 1$, whereas the real part of χ^0 is completely flat within the particle-hole continuum. By scaling the renormalized free susceptibility of the strong coupling limit, eq. (85), to $U = 3$ or $U = 6$ we obtain the dashed lines in Figs. 4, 5 and 6.

Substituting eq. (85) in eq. (64) yields the renormalized RPA response functions. The large U charge response is characterized by a small continuum within $|\xi| < 1$,

$$\text{Im } \chi^{\text{ch}}(\xi) = -\frac{2}{U} \frac{\xi \sqrt{1-\xi^2}}{4-3\xi^2}. \quad (86)$$

Outside the particle-hole continuum, the charge response has a collective pole at $\xi = 2/\sqrt{3}$, describing a undamped plasmon obeying the dispersion relation

$$\Omega_p = \frac{8}{\sqrt{3}} \left| \sin \frac{q}{2} \right|. \quad (87)$$

Notice that the dispersion relation of the renormalized plasmon becomes independent of U in the large U limit. The pure RPA, in contrast, predicts in this limit a plasmon dispersion proportional to U . The strong coupling charge response scaled to the appropriate U is represented in Fig. 9 and Fig. 10 by the dashed lines.

From the second of the eqs. (64), in combination with the renormalized free susceptibility (85), we obtain the large U spin response in renormalized RPA. It is fully described by a continuum for $|\xi| < 1$,

$$\text{Im } \chi^{\text{sp}}(\xi) = -\frac{1}{2U} \frac{\sqrt{1-\xi^2}}{\xi}, \quad (88)$$

and vanishes elsewhere. This is plotted with dashed lines in Fig. 11 for $U = 3$ and Fig. 12 for $U = 6$. No collective excitations occur, since the denominator of the renormalized RPA spin response, $1+U\chi^0$, is always finite. Nevertheless, we see from eq. (88) that the spin continuum diverges at $\omega = 0$ with consequences that we will discuss below.

It can be shown that the real and imaginary part of χ^0 from eq. (85) fulfill the Kramers-Kronig relations. Moreover, we will show in appendix C that the occupation numbers calculated from the large U expression of the renormalized RPA Green's function via the spectral theorem (53) are consistent with eq. (82). This means that the occupation numbers (82) fulfill together with the strong coupling susceptibilities (86) and (88) the self-consistency condition of the renormalized RPA.

The number of double occupancies per site are given by

$$\frac{1}{N} \sum_i n_{i\uparrow} n_{i\downarrow} = \langle n_{\uparrow} \rangle \langle n_{\downarrow} \rangle + \frac{w^c}{U}, \quad (89)$$

where w^c stands for the correlated potential energy per site,

$$w^c = \frac{U}{N^2} \sum_{kpq} \left\langle a_{k\uparrow}^\dagger a_{k+q\uparrow} a_{p+q\downarrow}^\dagger a_{p\downarrow} \right\rangle^c. \quad (90)$$

w^c is independent of U , since the large U Green's function scales with $1/U$.

Nevertheless, as the expectation value in eq. (90) can be obtained from the spectral theorem (54) by integrating the renormalized RPA Green's function over positive frequencies, the $1/\omega$ divergence of the spin response (88) makes the expectation value w^c diverge logarithmically. This means that both, the total potential energy per site and the number of doubly occupied sites are going to $-\infty$ as $U \rightarrow \infty$.

One way to correct these deficient results is to calculate the ground-state energy $E(U)$ from the kinetic energy $T(U)$, using the Hellmann–Feynman–Theorem³²,

$$E(U) = U \int_U^\infty dy \frac{T(y)}{y^2}. \quad (91)$$

The behaviour of the kinetic energy in the renormalized RPA can be obtained from the occupation numbers (82). For large U , this yields

$$T(U) = -\frac{4}{U}. \quad (92)$$

Again, only the prefactor differs from the exact result,

$$T^{\text{exact}}(U) = -\frac{8 \ln 2}{U}, \quad (93)$$

known from the large U expansion of the Bethe ansatz solutions^{22,33}.

Calculating the ground-state by eq. (91), our theory predicts

$$E(U) = -\frac{2}{U} \quad (94)$$

as $U \rightarrow \infty$. The large U expansion of the renormalized RPA ground-state energy of the half filled Hubbard chain is shown in Fig. 17 by the dashed line. For arbitrary interactions, the renormalized RPA ground-state energy calculated with the Hellmann–Feynman theorem is illustrated by the “x”-symbols. This compares reasonably well with the exact result, known from Bethe ansatz (continuous line) and its large U expansion (dot-dashed line).

We now have access to the potential energy as the difference between ground-state energy and kinetic energy. It thus behaves as $2/U$ for large U . This implies that the number of double occupancies vanishes as $2/U^2$ for strong interactions. In Fig. 18, the number of double occupancies at half filling is monitored as a function of U . We see that for small interactions, the renormalized RPA (“x”-symbols) reproduces the exact result (continuous line). For large interaction strengths, our theory matches the Bethe ansatz expansion, $-(4 \ln 2)/U^2$ (dot-dashed line), apart from the prefactor.

V. DISCUSSION, CONCLUSIONS AND OUTLOOK

In this work, we performed a first application of the Self-Consistent RPA (SCRPA) theory to the Hubbard model. In itself, the SCRPA is an approximation to the general Dyson Equation Approach (DEA) to correlation functions where the full (exact) mass operator is replaced by its instantaneous contribution. For the single particle Green's function this strategy leads to the standard Hartree–Fock theory. In analogy, it has been argued in the past that the SCRPA corresponds to a HF theory for fermion pair clusters. Recently, this theory has produced very interesting results in various domains of many-body physics^{6,7}.

Unfortunately, being a (non-linear) mean-field theory for non-local correlation functions, SCRPA is numerically very demanding. As a first step, we therefore had to proceed to further rather drastic simplifications. The latter consist in retaining correlations *only* in the single-particle occupation numbers. This approximation to SCRPA is

known in the literature as *renormalized* RPA^{2,34}. In spite of this, the essentials of the self-consistency and closure aspects remain intact. As a further virtue, the f -sum rule is shown to be fulfilled in Self-Consistent as well as in renormalized RPA. This also implies that the Goldstone theorem is fulfilled and symmetries are treated correctly.

We solved numerically the renormalized RPA equations for the one-dimensional single-band Hubbard model in the paramagnetic phase, for different fillings and interactions. Although we were aware of the difficulty of describing one dimensional models because of the extreme importance of quantum correlations⁶, there were multiple reasons for this choice. In a first place, the exact solution of Lieb and Wu⁸ provides a benchmark for our results, which, in higher dimensions, does not exist. As was argued in section III A, we expect the renormalized RPA to perform better with increasing dimensionality. Therefore, $1d$ can be considered as a “worst case check” for our approximation. The second reason is mainly technical: The self-consistency equation for the occupation numbers (53) illustrates that the numerical effort increases with the square of the spatial dimension. Therefore, the experience in $1d$ is desirable before attacking higher dimensions. In the last place, even in one dimension, we are able to test explicitly the essentials of our method and the convergence of the iteration cycle.

As expected, most of the particularities of the one-dimensional model, as e.g. Luttinger liquid behaviour away from half filling, could not be reproduced. The scenario predicted by our theory rather confirms the results which were obtained from methods designed for higher dimensional models, like e.g. the Hubbard-III approximation^{18,19}: For small U , we find a Fermi-liquid like metallic ground state. The system undergoes a Mott-Hubbard transition for an interaction slightly smaller than the bandwidth. The exact value of the critical interaction depends on the filling. For stronger interactions, our theory predicts an insulator for all fillings.

Despite these deficiencies, we obtain several interesting results. In the strong coupling regime of the half filled model, for example, we are able to express the central quantities of our theory analytically. The renormalized RPA momentum distribution function, given by eq. (82), agrees, apart from a prefactor, with the $n_k \propto \cos k$ behaviour known from the large U expansion of the Bethe ansatz solution.

Moreover, the mean-field spin instability around $2k_F$, which causes the breakdown of the pure RPA for any finite interaction, turns out to be cured in renormalized RPA in the sense that no more purely imaginary eigenfrequencies occur in the spin channel. On the other hand, the renormalization is still rather weak such that a strongly overdamped spin pole remains at low energy. These low-lying spin excitations give rise to a slow (logarithmic) divergence of the two-body correlation functions, which is carried into the number of double occupancies and thus also into the ground-state energy. The stronger renormalization contained in the SCRPA would certainly cure this pathology, since it also renormalizes (screens) the interaction self-consistently. In this sense, the SCRPA bears some similarities with the approach of Tremblay et al.³⁵.

Several of the renormalized RPA results may nonetheless be improved by applying the Hellmann-Feynman theorem. Using this approach, which may simulate a step towards the full solution of the SCRPA, the ground-state energy compares for all interaction strengths reasonably well with the exact results, known from Bethe ansatz. Moreover, the number of doubly occupied sites shows a qualitatively correct behaviour over the whole U range. Especially for $U \rightarrow 0$, the mean-field value is recovered, and, for $U \rightarrow \infty$, the double occupancies vanish like $1/U^2$, as predicted by the exact solution.

In the strong coupling regime of the half filled model, this approach reproduces the exact results for the momentum distribution function, the ground-state energy, the kinetic and potential energy, and the number of doubly occupied sites, apart from a general prefactor. We would obtain the right prefactor by substituting the bare Hubbard U with a screened interaction, or, in other words, by multiplying U in our theory by a factor $1/(2 \ln 2) \approx 0.72$.

Since in renormalized RPA the Hubbard interaction is approximated by a simple spin-flip interaction, it is not astonishing that the best results are produced at half filling²³. Away from half filling, other scattering processes, still taken into account in SCRPA but neglected in renormalized RPA, become important. Therefore, the renormalized RPA is less effective. The Luttinger liquid behaviour, exhibited by the exact momentum distribution even for $U \rightarrow \infty$ ²⁵, is not obtained. In the strong coupling limit, the renormalized RPA produces smooth occupation numbers, although still having a steeper slope at k_F as at half filling. For small interactions, the renormalized RPA still predicts a discontinuity in the momentum distribution at k_F . This implies that the Luttinger theorem is satisfied.

A further point to be discussed is the fact that we completely neglected the dynamical interaction part, $\mathcal{H}_{AB}^{\text{res}}(\omega)$, defined in eq. (11). It is certainly true, as recently pointed out by Logan for the infinite dimensional Hubbard model³⁶, that this dynamical interaction should be taken into account, in order to describe the low energy scale in the spin channel correctly. Nevertheless, in the present work, some dynamical effects in the spin channel are considered via the coupling of the occupation numbers to the RPA ground state correlations. A full inclusion of the dynamical effects goes, however, beyond the scope of this paper.

At this point, it may be appropriate to shortly come back to some technical aspects of the SCRPA which we did not develop in the main text in order not to overduely extend the size of the paper. In the introduction, we mentioned that the Equation of Motion Method (EOM), on which our formalism is based, goes back rather far in time. The first major theoretical input was developed by D.J. Rowe in his review article², where the calculation of density-

density correlation functions is described in the context of nuclear physics. The method was later applied to strongly correlated electrons by Roth³. She evaluated the single-particle Green's function by coupling it in an approximate way to the three particle propagator (see also Beenen and Edwards³⁷ for a more recent application to the Hubbard model). Since then, in solid state physics, the EOM has, to the best of our knowledge, exclusively been used for the calculation of single particle properties³⁸.

As we point out in ref.⁹, the optimal procedure will be to combine single-particle and fermion-pair channels. Indeed, as is well known, the single particle mass operator can be expressed exactly by the two-particle T -matrix³⁹. Replacing it by its SCRPA counterpart then naturally leads to a self-consistent coupling of both channels. In this scheme, as we will describe in more detail in a future publication, the single-particle occupation numbers will not be evaluated from the particle-hole propagator (see eqs. (27) and (53), respectively) but directly from the single-particle Green's function. A further advantage of this strategy is that single-particle and fermion-pair properties are obtained simultaneously and on equal footing. We did not follow this route in this paper, since it again would have strongly increased the numerical difficulties. In spite of these possible improvements, the present investigation shows that the essentials of the SCRPA theory (i.e. the self-consistency procedure) work correctly in a numerical application to a homogeneous system of strongly interacting fermions. Once the method will be solvable in its full complexity, the possible applications are very numerous. Indeed, the SCRPA is a very flexible formalism applicable to strongly correlated Fermi systems, but also to Bose or spin systems. The study of such systems are planned in the future.

A very appealing application of the SCRPA may be the Hubbard model in infinite dimensions, since, on one hand, the physics in $d = \infty$ is expected to be somewhat similar to $d = 3$. On the other hand, spatial fluctuations are suppressed in $d = \infty$ which allows to reduce the many-body problem to either a dynamical single-site problem, or, to an effective one dimensional problem. We thus may expect, that the numerical solution of the SCRPA will be feasible in infinite dimensions, in contrast to finite dimensions, where the effort will grow with an exponent $3d$, since the effective Hamiltonian contains correlation function depending on three momenta.

ACKNOWLEDGMENTS

We are specially grateful to Florian Gebhard for many interesting discussions and stimulating comments, and the careful reading of the manuscript. We also thank Jorge Dukelsky, Mireille Lavagna and Wilhelm Brenig for criticism and many helpful comments.

APPENDIX A: DERIVATION OF THE SCRPA FROM A VARIATIONAL PRINCIPLE

In this section, we will briefly outline the derivation of the particle-hole SCRPA equations from a variational principle. An analogous method was derived by Baranger⁴⁰ for the single particle case.

Let us therefore consider the spectral representation of the retarded Green's function

$$\langle\langle X; X^+ \rangle\rangle_{\omega}^{\text{ret}} = \sum_n \left[\frac{\langle 0|X|n\rangle\langle n|X^+|0\rangle}{\omega - \omega_{n0} + i0^+} - \epsilon \frac{\langle 0|X^+|n\rangle\langle n|X|0\rangle}{\omega + \omega_{n0} + i0^+} \right], \quad (\text{A1})$$

where $|0\rangle$ is the exact ground state of H , and ω_{n0} denotes the excitation energy for the exact eigenstates $|n\rangle$. For the particle-hole problem, we set $\epsilon = +1$. The excitation operators X^+ are given by

$$X^+ = \sum_{kp} x_{kp} a_k^+ a_p. \quad (\text{A2})$$

The normalized mean excitation energy is given by:

$$\begin{aligned} S_1 &= \frac{\sum_n \omega_{n0} \left(|\langle n|X^+|0\rangle|^2 - |\langle n|X|0\rangle|^2 \right)}{\sum_n \left(|\langle n|X^+|0\rangle|^2 - |\langle n|X|0\rangle|^2 \right)} \\ &= \frac{\int_{-\infty}^{\infty} d\omega \omega \text{Im} \langle\langle X; X^+ \rangle\rangle_{\omega}^{\text{ret}}}{\int_{-\infty}^{\infty} d\omega \text{Im} \langle\langle X; X^+ \rangle\rangle_{\omega}^{\text{ret}}} \end{aligned} \quad (\text{A3})$$

The equivalence between the first and the second line can be seen by substituting the spectral representation (A1) in the second line. The denominator can easily be evaluated with the spectral theorem (15). This yields the norm $\langle 0|[X, X^+]|0\rangle$, which would be equal to unity if X^+ were ideal bose operators.

We now minimize eq. (A3) with respect to the excitation operators. The X^+ with the lowest mean excitation energy obey the condition:

$$\frac{\partial S_1}{\partial x_{kp}} = 0 \quad (\text{A4})$$

It is straightforward to verify that eq. (A4) leads to the SCRPA for the particle-hole propagator derived in section II C.

APPENDIX B: FREE SUSCEPTIBILITY IN ONE DIMENSION

The free susceptibility is obtained by performing the integral in eq. (61) for step-like occupation numbers (63). Because of the symmetry of the dispersion relation ε_k , the real part of $\chi^0(q, \omega)$ is symmetric in q and ω , whereas the imaginary part is symmetric in q and antisymmetric in ω .

In the paramagnetic phase, $n_{k\uparrow} = n_{k\downarrow}$, and in one dimension, the explicit expression for the real part is:

$$\begin{aligned} \text{Re } \chi^0(q, \omega) = \frac{1}{\pi\sqrt{|z|}} & \left[\text{atan} \left(\frac{\sqrt{|z|} \sin k_F}{\omega \cos k_F - 4 \sin^2(q/2)} \right) \right. \\ & \left. - \text{atan} \left(\frac{\sqrt{|z|} \sin k_F}{\omega \cos k_F + 4 \sin^2(q/2)} \right) \right] \end{aligned} \quad (\text{B1})$$

with $z = (4 \sin \frac{q}{2})^2 - \omega^2$ and

$$\text{atan } x = \begin{cases} \arctan x & \text{for } z < 0 \\ \text{artanh } x & \text{for } z > 0 \text{ and } |x| < 1 \\ \text{arcoth } x & \text{for } z > 0 \text{ and } |x| > 1 \end{cases} \quad (\text{B2})$$

For the imaginary part, we find in agreement with B enard et al.⁴¹

$$\begin{aligned} \text{Im } \chi^0(q, \omega) = -\frac{\Theta(z)}{2\sqrt{|z|}} & \left[\Theta \left(\varepsilon_F + \frac{\omega}{2} + \frac{1}{2}\sqrt{|z|} \cot \frac{q}{2} \right) \right. \\ & + \Theta \left(\varepsilon_F + \frac{\omega}{2} - \frac{1}{2}\sqrt{|z|} \cot \frac{q}{2} \right) \\ & - \Theta \left(\varepsilon_F - \frac{\omega}{2} + \frac{1}{2}\sqrt{|z|} \cot \frac{q}{2} \right) \\ & \left. - \Theta \left(\varepsilon_F - \frac{\omega}{2} - \frac{1}{2}\sqrt{|z|} \cot \frac{q}{2} \right) \right]. \end{aligned} \quad (\text{B3})$$

APPENDIX C: SELF-CONSISTENCY OF THE LARGE U LIMIT

In this section, we will briefly outline that the occupation numbers which are given by eq. (82) for the half filled Hubbard chain in the large U limit are indeed a fully self-consistent solution of the renormalized RPA equations.

If we assume the occupation numbers from eq. (82), we find the renormalized free susceptibility (85) by calculating the k -sum in eq. (61). The large U limit of the renormalized RPA Green's functions is then obtained by substituting $\chi^0(q, \omega)$ in eq. (62).

We are now able to calculate a new set of occupation numbers by inserting this renormalized RPA Green's function in eq. (53). For convenience, however, we will rather use the commutator spectral theorem, eq. (15), itself:

$$\begin{aligned}
(n_{k\sigma} - n_{k+q\sigma})^{\text{new}} &= -\frac{1}{\pi} \sum_p \int_{-\infty}^{\infty} d\omega \operatorname{Im} \mathcal{G}_{k\sigma p\sigma}(q, \omega) \\
&= -\frac{1}{\pi} \int_{-\infty}^{\infty} d\omega \operatorname{Im} \left[\frac{(n_{k\sigma} - n_{k+q\sigma})^{\text{old}}}{\omega - [\varepsilon_{k+q} - \varepsilon_k] + i0^+} \frac{1}{1 - U\chi_{\uparrow}^0(q, \omega) U\chi_{\downarrow}^0(q, \omega)} \right]
\end{aligned} \tag{C1}$$

For the self-consistency to be fulfilled, we now have to show that the “new” occupation numbers are equal to the “old” ones. As we are in the paramagnetic phase, we may drop the spin indices and convert the integrand in a partial fraction. After substituting $x = \omega/|4 \sin \frac{q}{2}|$ and $y_{kq} = [\varepsilon_{k+q} - \varepsilon_k]/|4 \sin \frac{q}{2}|$, we find for the ratio between new and old occupation numbers:

$$I(y_{kq}) = -\frac{1}{2\pi} \int_{-\infty}^{\infty} dx \operatorname{Im} \left[\frac{1}{x - y_{kq} + i0^+} \left(\frac{1}{1 - U\chi^0} + \frac{1}{1 + U\chi^0} \right) \right] \tag{C2}$$

In the following, we will treat the two fractions in the integrand separately, considering in analogy to eq. (64) the first term as the charge term, and the second term as the spin term. With the renormalized free susceptibility from eq. (85), the denominator of the charge term may be written as

$$1 - U\chi^0(x) = \begin{cases} 2 + i\frac{x}{\sqrt{1-x^2}} & \text{for } |x| < 1 \\ 2 - \frac{|x|}{\sqrt{x^2-1}} + i0^+ \operatorname{sign} x & \text{for } |x| > 1 \end{cases} . \tag{C3}$$

In the same way, the denominator of the spin term is

$$1 + U\chi^0(x) = \begin{cases} -i\frac{x}{\sqrt{1-x^2}} & \text{for } |x| < 1 \\ \frac{|x|}{\sqrt{x^2-1}} - i0^+ \operatorname{sign} x & \text{for } |x| > 1 \end{cases} . \tag{C4}$$

To solve the integral, we have to account for three different contributions: The first one comes from the pole of the free ph Green’s function, $1/(x - y_{kq} + i0^+)$, which lies always in the ph continuum, i.e. $|y_{kq}| \leq 1$. With Dirac’s identity,

$$\frac{1}{f(x) \pm i0^+} = \mathcal{P} \frac{1}{f(x)} \mp i\pi\delta[f(x)] , \tag{C5}$$

we find for the charge contribution

$$I_1^{\text{ch}}(y_{kq}) = \frac{1 - y_{kq}^2}{4 - 3y_{kq}^2} . \tag{C6}$$

The corresponding spin contribution is zero, since $1 + U\chi^0(x)$ is purely imaginary within the ph continuum.

Secondly, we have to integrate over the charge and spin continuum, respectively. Therefore, we combine the imaginary part of $1/(1 \pm U\chi^0)$ with the real part of the free ph Green’s function. This yields

$$\begin{aligned}
I_2^{\text{ch}}(y_{kq}) &= \frac{2 - 3y_{kq}^2}{6(4 - 3y_{kq}^2)} \\
I_2^{\text{sp}}(y_{kq}) &= \frac{1}{2}
\end{aligned} \tag{C7}$$

The last contribution comes from the collective poles. Again, the spin contribution is zero, as the renormalized spin response does not show any magnon peak in the strong coupling limit. As pointed out in section IV G, the plasmon peak occurs at $x = \pm 2/\sqrt{3}$. Using the Dirac identity (C5) once more, we get

$$I_3^{\text{ch}}(y_{kq}) = \frac{2}{3(4 - 3y_{kq}^2)} . \tag{C8}$$

Summing the three contributions, (C6), (C7) and (C8), yields unity for the ratio of the new and the old occupation numbers, $I(y_{kq})$. By this means, we have found a fully self-consistent solution of the renormalized RPA equations.

- ¹ J.P. Blaizot, G. Ripka, *Quantum Theory of Finite Systems*, The MIT Press, Cambridge, 1986.
- ² For a review of older literature see D.J. Rowe, *Rev. Mod. Phys.* **40** 153 (1968).
- ³ L.M. Roth, *Phys. Rev.* **184** 451 (1969).
- ⁴ J. Dukelsky, P. Schuck, *Nucl. Phys. A* **512** 466 (1990).
- ⁵ G. Röpke, *Ann. Physik (Leipzig)* **3**, 145 (1994); G. Röpke, *Z. Phys. B.* **99**, 83 (1995).
- ⁶ P. Krüger, P. Schuck, *Europhys. Lett.* **72**, 395 (1994).
- ⁷ J. Dukelsky, P. Schuck, *Mod. Phys. Lett. A* **26** 2429 (1991); J. Dukelsky, P. Schuck, *Phys. Lett. B* **387** 233 (1996).
- ⁸ E.H. Lieb, F.Y. Wu, *Phys. Rev. Lett.* **20**, 1445 (1968).
- ⁹ J. Dukelsky, G. Röpke, P. Schuck, *Nucl. Phys. A* **628**, 17 (1998).
- ¹⁰ P. Ring, P. Schuck, *The Nuclear Many-Body Problem*, Springer, Berlin 1980.
- ¹¹ W. Nolting, *Grundkurs Theoretische Physik, 7. Viel-Teilchen-Theorie*, Zimmermann-Neufang, 1992.
- ¹² R. Kubo, *Jour. Phys. Soc. Japan* **17**, 1100 (1962).
- ¹³ J.W. Negele, H. Orland, *Quantum Many-Particle Systems*, Addison-Wesley, 1988.
- ¹⁴ J. Hubbard, *Proc. Roy. Soc. A* **240**, 539 (1957); **243**, 336 (1958); **276**, 238 (1963).
- ¹⁵ W.F. Brinkman, T.M. Rice *Phys. Rev. B* **2**, 1324 (1970); see also F. Gebhard¹⁷.
- ¹⁶ N.D. Mermin and H. Wagner, *Phys. Rev. Lett.* **17**, 1133 (1966).
- ¹⁷ F. Gebhard, *The Mott Metal Insulator Transition*, Springer Tracts in Modern Physics, Vol. 137 (1997).
- ¹⁸ J. Hubbard, *Proc. Roy. Soc. A* **281**, 401 (1964).
- ¹⁹ M. Cyrot, *Physica B* **91**, 141 (1977).
- ²⁰ D.J. Thouless, *Nucl. Phys.* **22**, 78 (1961).
- ²¹ S. Sorella, A. Parola, M. Parinello, E. Tosatti, *Europhys. Lett.* **12** (8), 721 (1990).
- ²² J. Carmelo, D. Baeriswyl, *Phys. Rev. B* **37**, 7541 (1988).
- ²³ D. Baeriswyl, W. von der Linden in *The Hubbard Model - Recent Results*, ed. by M. Rasetti, (World Scientific, Singapore, 1991).
- ²⁴ A.B. Migdal, *Sov. Phys. JETP* **5**, 333 (1957), J.M. Luttinger and J.C. Ward, *Phys. Rev.* **118**, 1417 (1960), J.M. Luttinger *Phys. Rev.* **119**, 1153 (1960), *ibid.* **121**, 942 (1961).
- ²⁵ M. Ogata, H. Shiba in *Technical Report of ISSP*, published by The Institute of Solid State Physics, The University of Tokyo, Ser. A, No. 2189, (1989).
- ²⁶ M. Ogata, T. Sugiyama, and H. Shiba, *Phys. Rev. B* **43**, 8401 (1991); M. Ogata, H. Shiba *ibid.* **41**, 2326 (1990).
- ²⁷ K. Penc, F. Mila, H. Shiba, *Phys. Rev. Lett.* **75**, 894 (1995).
- ²⁸ M. Dzierzawa in *The Hubbard Model: Its Physics and Mathematical Physics*, ed. by D. Baeriswyl, D.K. Campbell, J.M.P. Carmelo, F. Guinea, and E. Louis, NATO ASI Series B **343**, (Plenum Press New York, 1995), p327.
- ²⁹ S. Sorella, E. Tosatti, S. Baroni, R. Car, M. Parinello, *Int. J. Mod. Phys. B* **1**, 993 (1988).
- ³⁰ J. Voit, *Reports on Progress in Physics* **58**, 977 (1995).
- ³¹ E.C. Stoner, *Journal de Phys. et Rad.* **12**, 372 (1951).
- ³² C. Kittel, *Quantum Theory of Solids*, John Wiley & Sons, 1987.
- ³³ D. Baeriswyl, J. Carmelo, A. Luther, *Phys. Rev. B* **33**, 7247 (1986); **34**, 8976(E) (1986).
- ³⁴ J. Toivanen, J. Suhonen, *Phys. Rev. C* **55**, 2314 (1997).
- ³⁵ Y.M. Vil'k, L. Chen, A.-M.S. Tremblay, *Phys. Rev. B* **49**, 13 267 (1994); *ibid.* *Physica C* **235-240**, 2235 (1994).
- ³⁶ D.E. Logan, M.P. Eastwood, M.P. Tusch, *Phys. Rev. Lett.* **76**, 4785 (1996); *ibid.* *J. Phys.: Condens. Matter* **9**, 4211 (1997); *ibid.* *J. Phys.: Condens. Matter* **10**, 2673 (1998).
- ³⁷ J. Beenen, D.M. Edwards, *Phys. Rev. B* **52**, 13 636 (1995).
- ³⁸ A.L. Kuzemsky, J.C. Parlebas, H. Beck, *Physica A* **198** 606 (1993).
- ³⁹ A.B. Migdal, *Theory of Finite Fermi Systems and Applications to Atomic Nuclei*, Monographs and Texts in Physics and Astronomy, Interscience Publishers, a division of John Wiley & Sons, New York (1967).
- ⁴⁰ M. Baranger, *Nucl. Phys. A* **149**, 225 (1970).
- ⁴¹ P. Bénard, L. Chen, A.-M.S. Tremblay, *Phys. Rev. B* **47**, 15217 (1993).

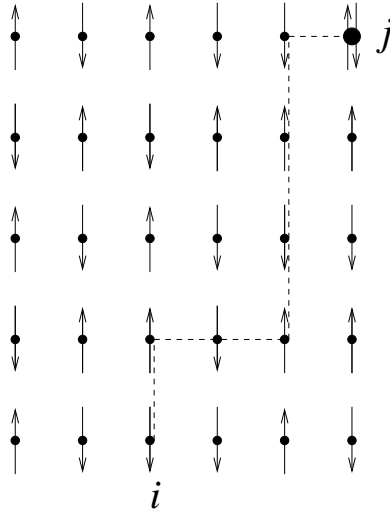


FIG. 1. An electron propagating in an antiferromagnetic lattice from site i to site j

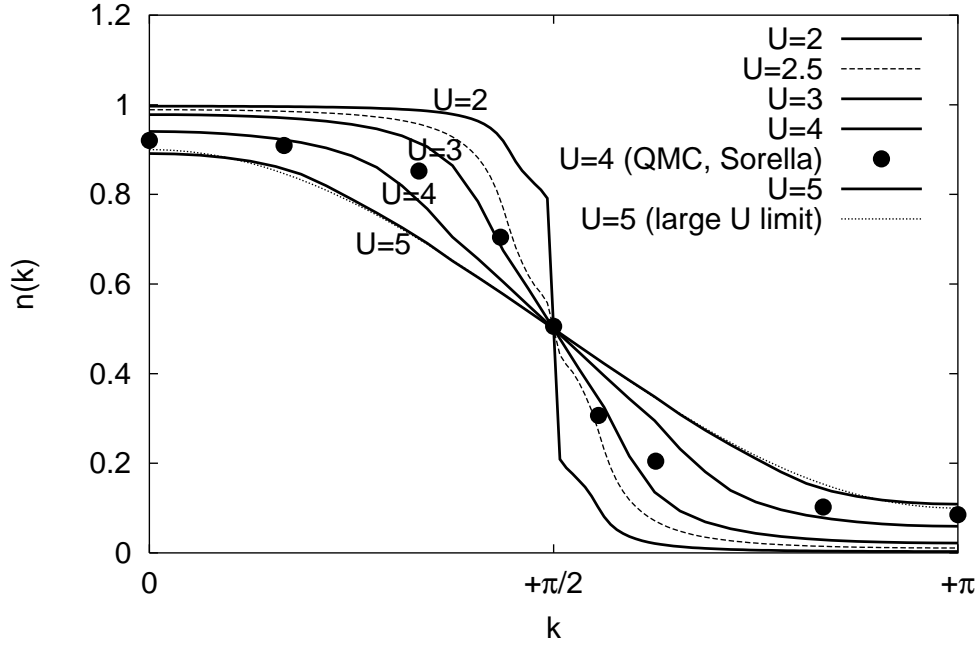


FIG. 2. Momentum distribution function n_k for the half-filled Hubbard chain. Quantum Monte-Carlo data from Sorella²⁹. The dotted line shows the large U limit of the renormalized RPA, given by eq. (82).

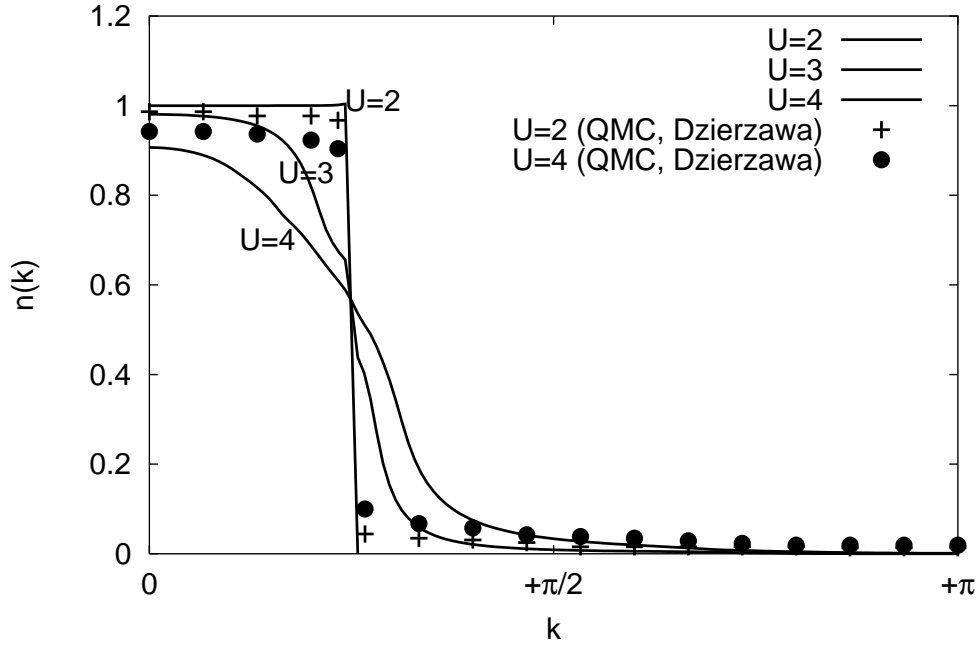


FIG. 3. Momentum distribution function n_k for the quarter-filled Hubbard chain. Quantum Monte-Carlo data from Dzierzawa²⁸.

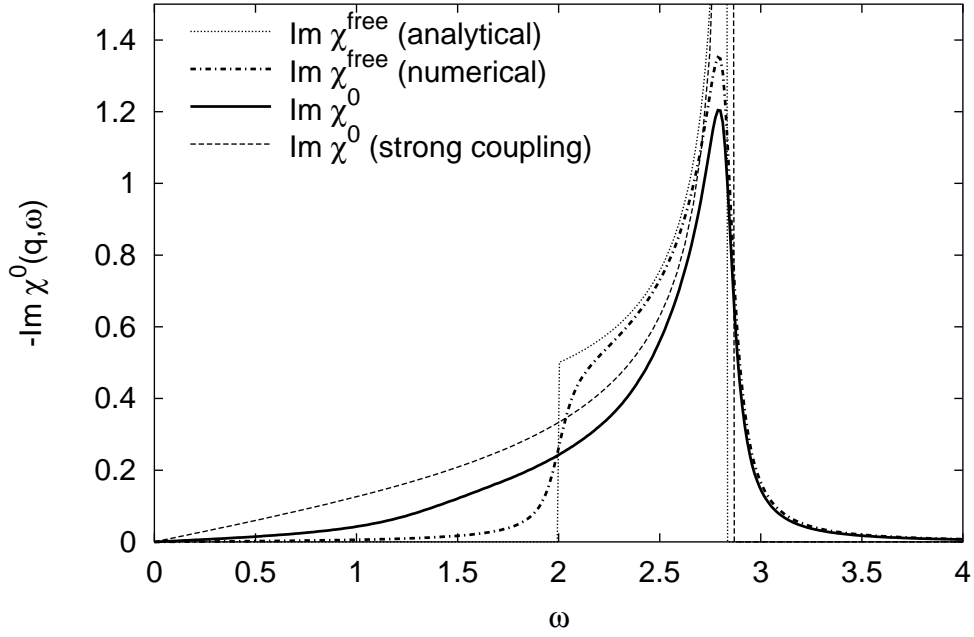


FIG. 4. Imaginary part of the free and renormalized free susceptibility $\chi^0(q = \pi/2, \omega)$ for the half filled Hubbard chain at $U = 3$.

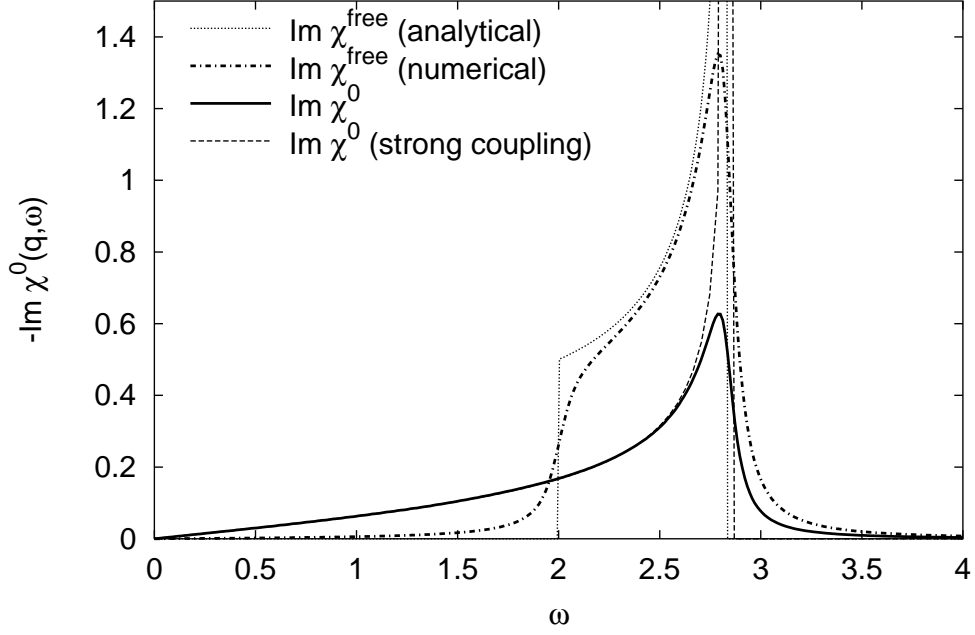


FIG. 5. Imaginary part of the free and renormalized free susceptibility $\chi^0(q = \pi/2, \omega)$ for the half filled Hubbard chain at $U = 6$.

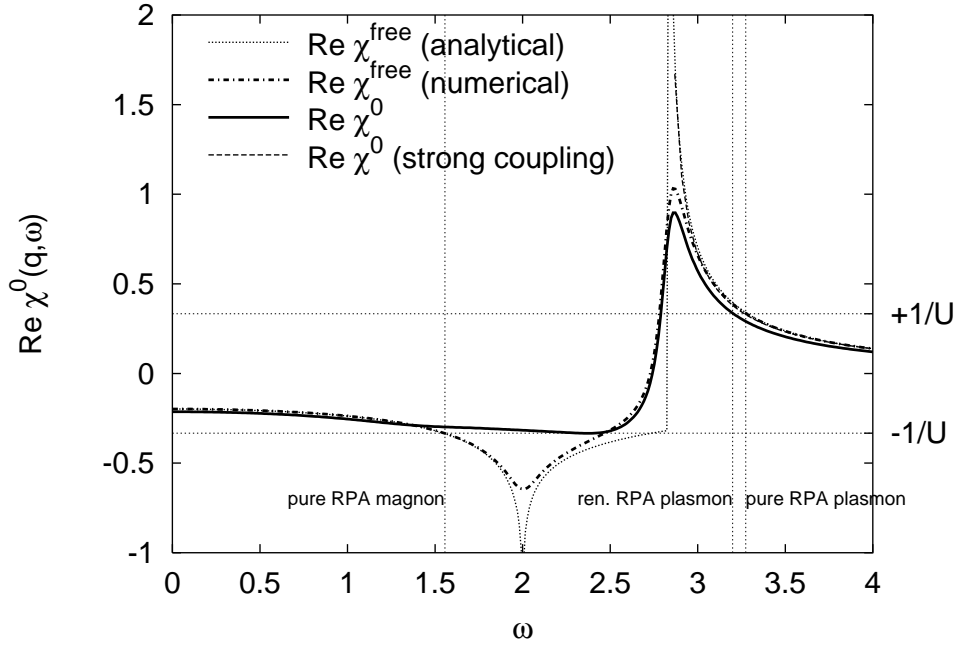


FIG. 6. Real part of the free and renormalized free susceptibility $\chi^0(q = \pi/2, \omega)$ for the half filled Hubbard chain at $U = 3$. The intersection with the horizontal lines at $\pm 1/U$ indicate where the collective excitations occur (see text).

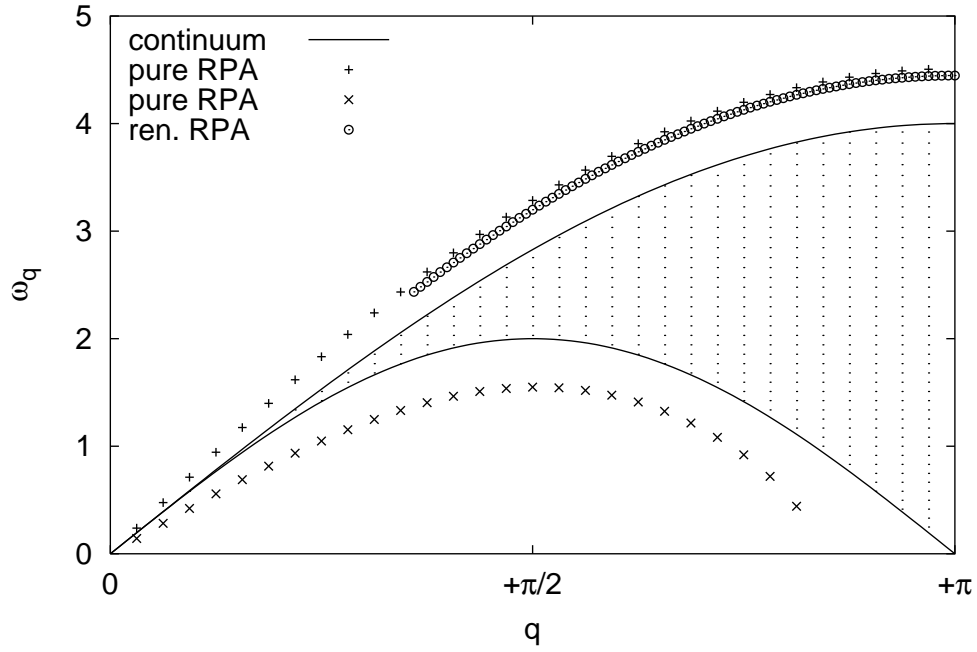


FIG. 7. Plasmon and magnon dispersion for the half filled Hubbard chain at $U = 3$. The renormalized RPA plasmons are plotted with circles. “+”- and “x”-symbols stand for the pure RPA plasmons and magnons, respectively. The dotted area illustrates the non-interacting particle-hole continuum. Its boundaries are given by the continuous lines.

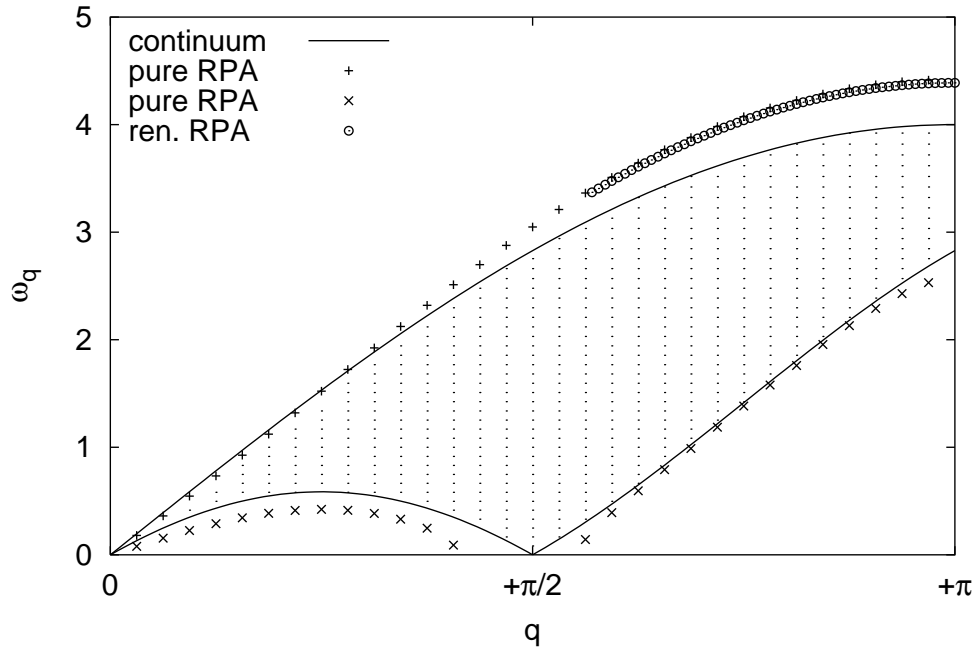


FIG. 8. Plasmon and magnon dispersion for the quarter filled Hubbard chain at $U = 3$. Symbols as in Fig. 7.

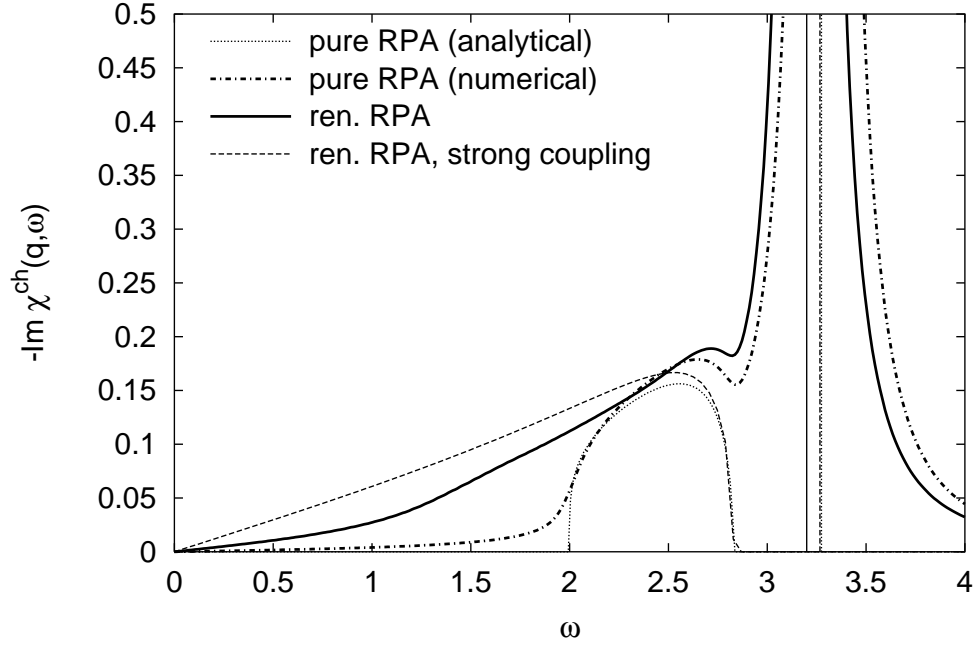


FIG. 9. Charge response $\chi^{\text{ch}}(q = \pi/2, \omega)$ in pure and renormalized RPA for the half filled Hubbard chain at $U = 3$. The vertical lines indicate the plasmon peaks. Accidentally, the pure RPA plasmon and the strong coupling plasmon occur at almost the same energy, such that the dotted and the dashed vertical line cannot be resolved from another. The thin continuous vertical line illustrates the precise position of the renormalized RPA plasmon, which itself is represented by the singularity in the renormalized RPA charge response (continuous line).

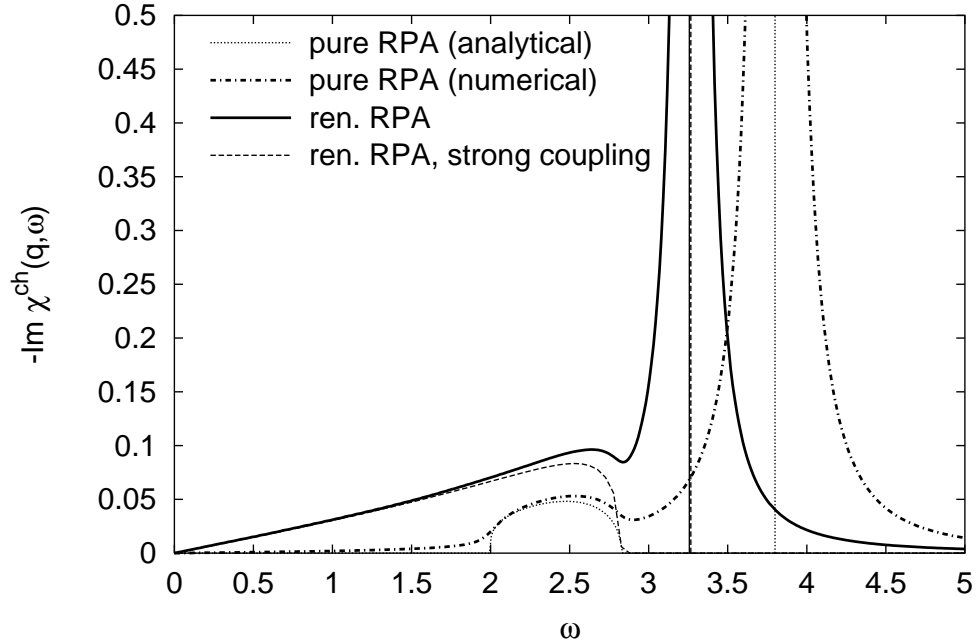


FIG. 10. Charge response $\chi^{\text{ch}}(q = \pi/2, \omega)$ in pure and renormalized RPA for the half filled Hubbard chain at $U = 6$. The vertical lines indicate the plasmon peaks (see Fig. 9). The strong coupling limit of our theory is reached, and the renormalized RPA plasmon (continuous vertical line) cannot be resolved from the strong coupling plasmon (dashed vertical line).

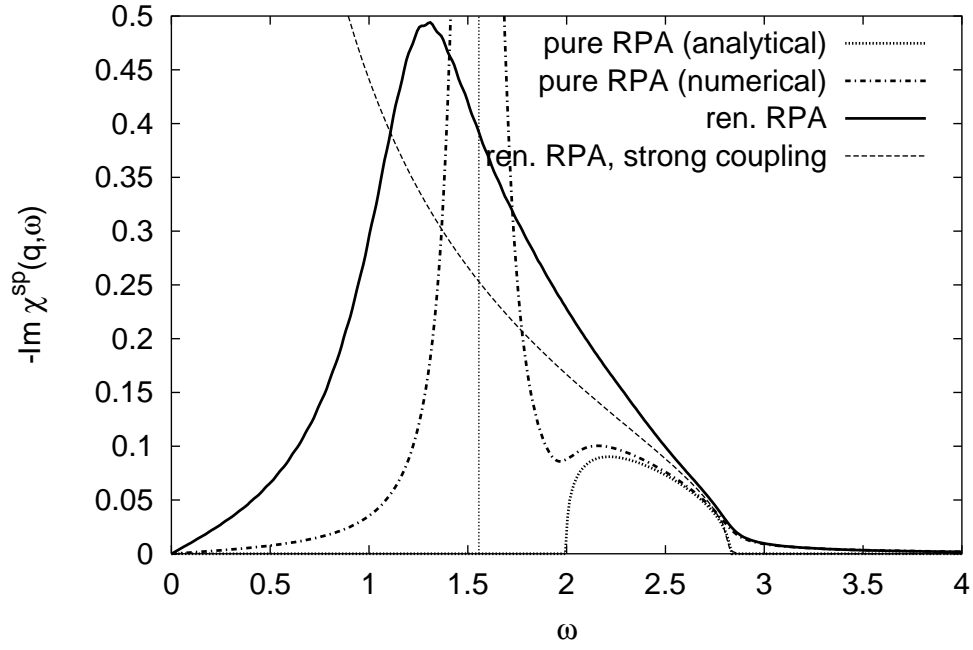


FIG. 11. Spin response $\chi^{\text{SP}}(q = \pi/2, \omega)$ in pure and renormalized RPA for the half filled Hubbard chain at $U = 3$. The vertical line indicates the pure RPA magnon peak.

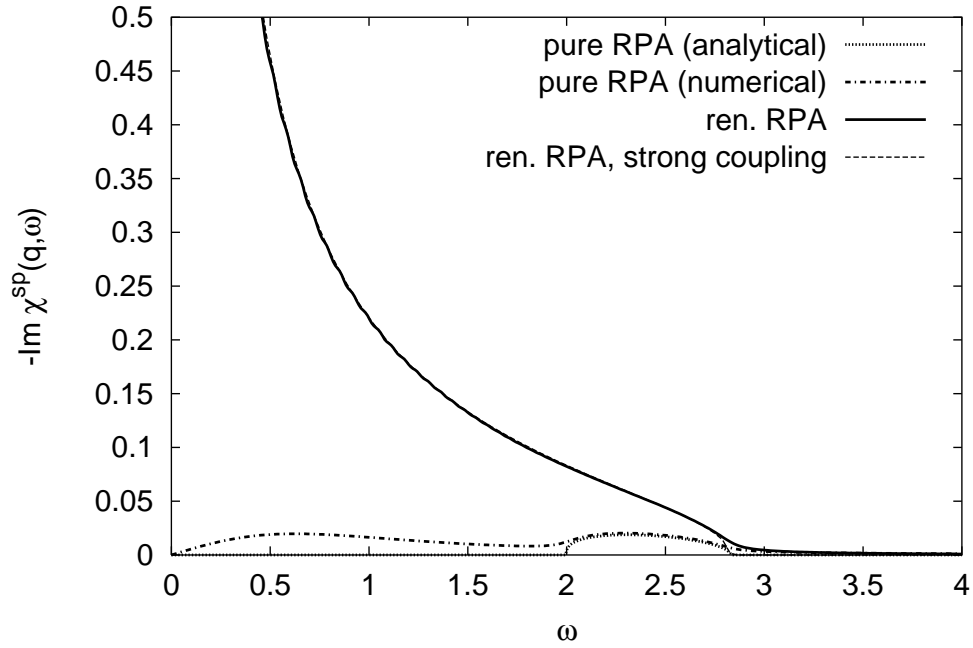


FIG. 12. Spin response $\chi^{\text{SP}}(q = \pi/2, \omega)$ in pure and renormalized RPA for the half filled Hubbard chain at $U = 6$. The magnon peak, present in Fig. 11, has vanished due to the instability of the pure RPA (see text).

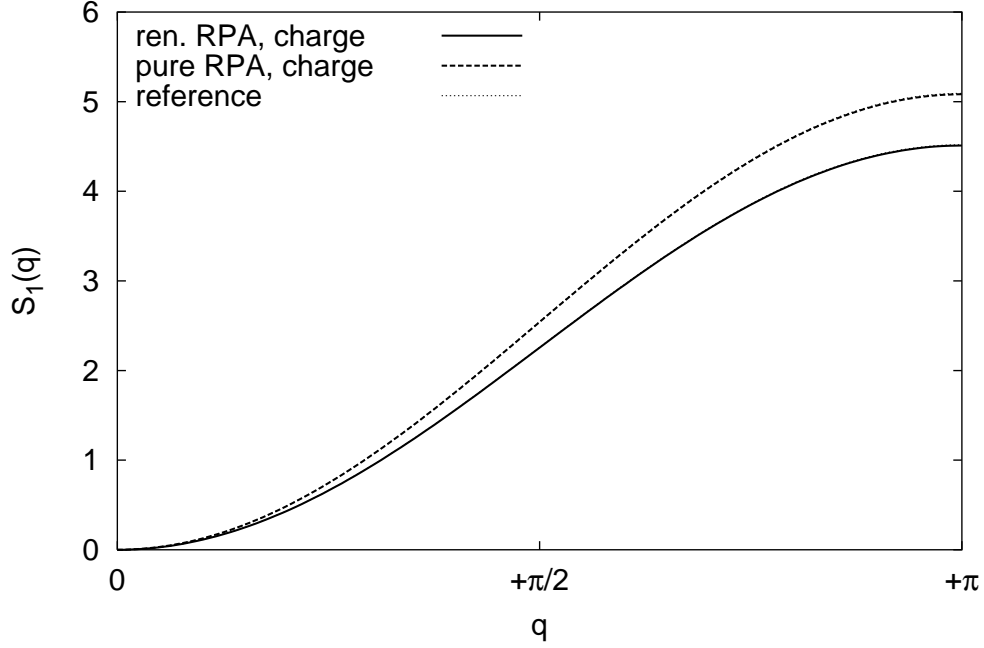


FIG. 13. Energy weighted sum rule for the renormalized and pure RPA charge susceptibility for the half filled Hubbard chain at $U = 3$. The dashed and continuous line correspond to the rhs. of the charge sum rule $S_1^{\text{ch}}(q)$, eq. (81), computed with the pure and renormalized RPA charge susceptibility, respectively. The left hand side of the sum rule is plotted with the thin dotted “reference” lines. As the sum rule is fulfilled in both cases, these reference lines cannot be resolved from the corresponding continuous or dashed lines.

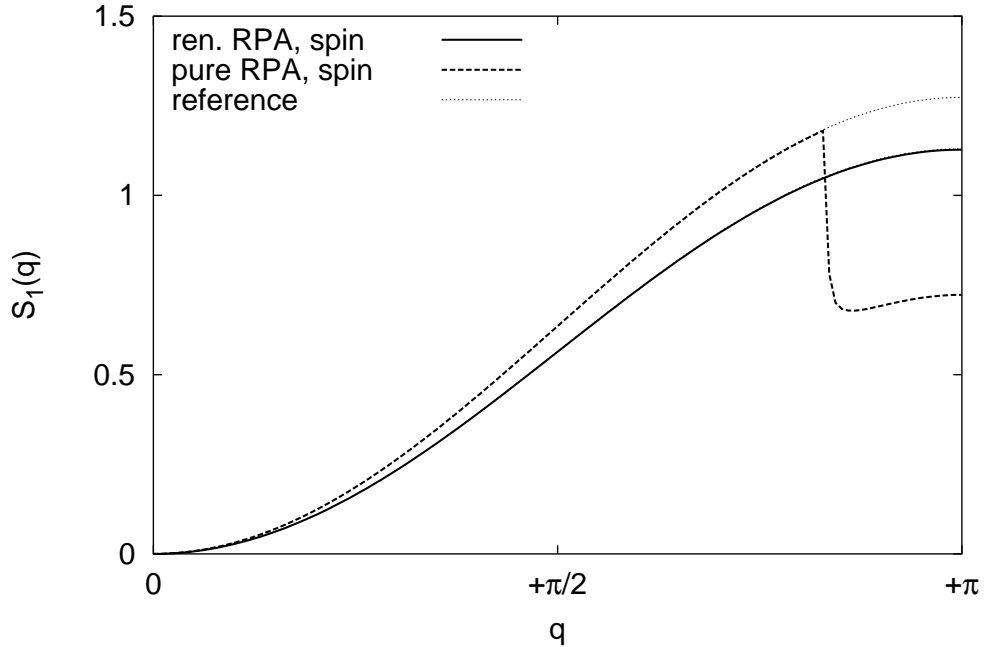


FIG. 14. Energy weighted sum rule for the longitudinal spin susceptibility in renormalized and in pure RPA for the half filled Hubbard chain at $U = 3$. The dashed and continuous line correspond to the rhs. of the spin sum rule $S_1^{\text{sp}}(q)$, eq. (81), computed with the pure and renormalized RPA spin susceptibility, respectively. The left hand side of the sum rule is plotted with the thin dotted “reference” lines. As the sum rule for the renormalized RPA is fulfilled, the reference line cannot be resolved from the continuous line. For the pure RPA, there is a region around $2k_F$ where the sum rule breaks down.

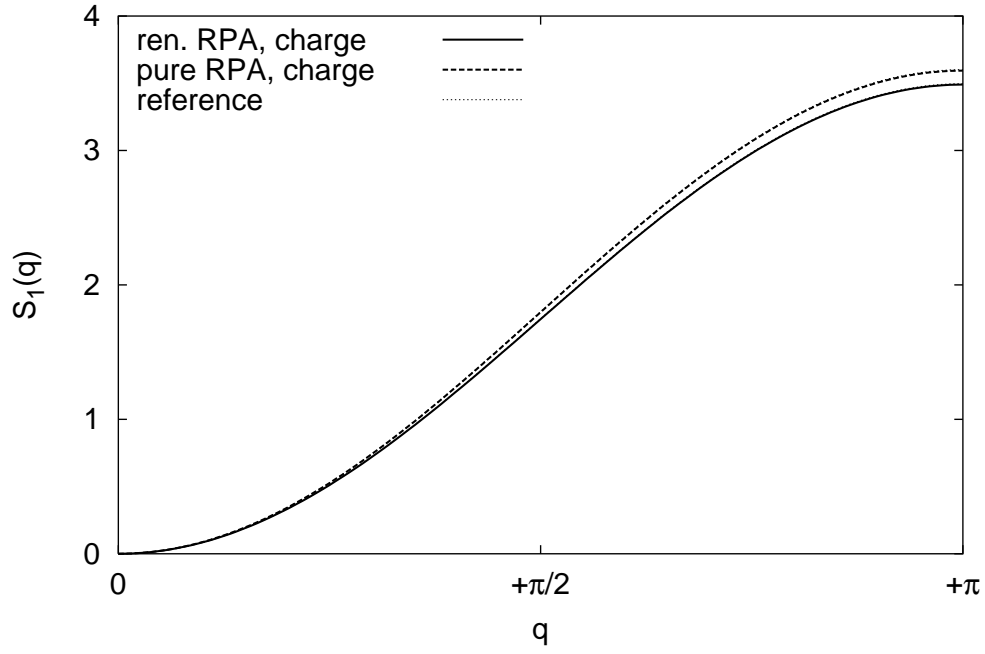


FIG. 15. Energy weighted sum rule for the renormalized and pure RPA charge susceptibility for the quarter filled Hubbard chain at $U = 3$. Description as in Fig. 13.

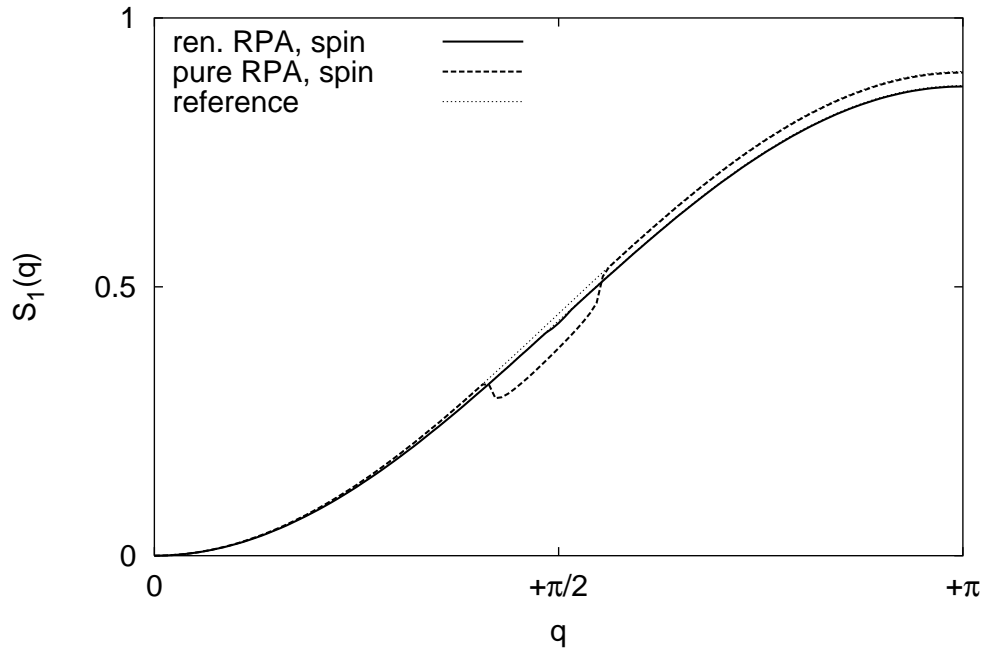


FIG. 16. Energy weighted sum rule for the longitudinal spin susceptibility in renormalized and in pure RPA for the quarter filled Hubbard chain at $U = 3$. Description as in Fig. 14.

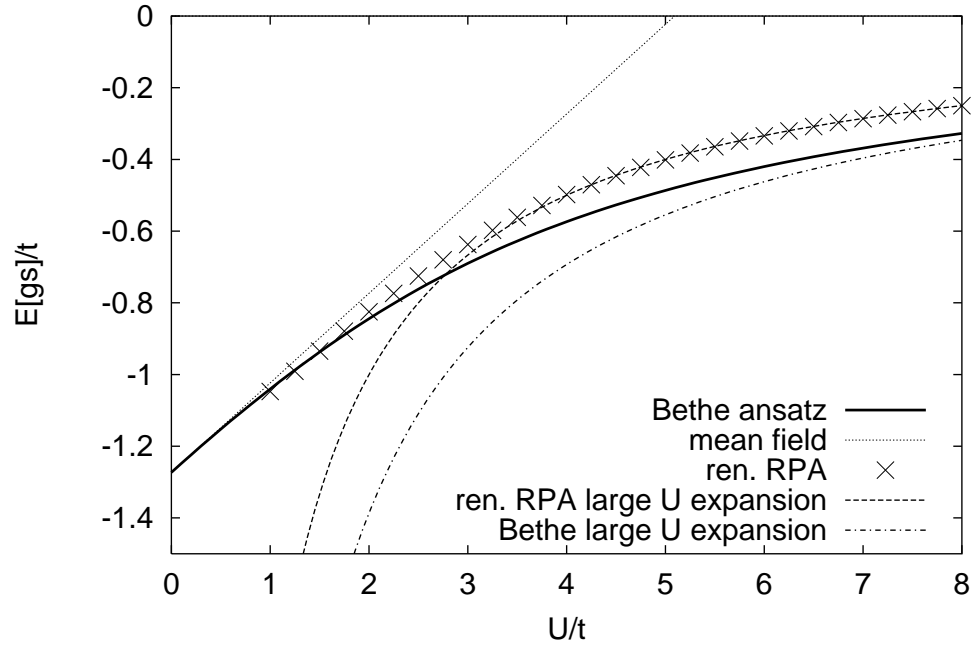


FIG. 17. Ground state energy per site for the half filled Hubbard chain. Bethe ansatz expansion from Baeriswyl et al.^{33,22}. Large U limit of the renormalized RPA from eq. (94).

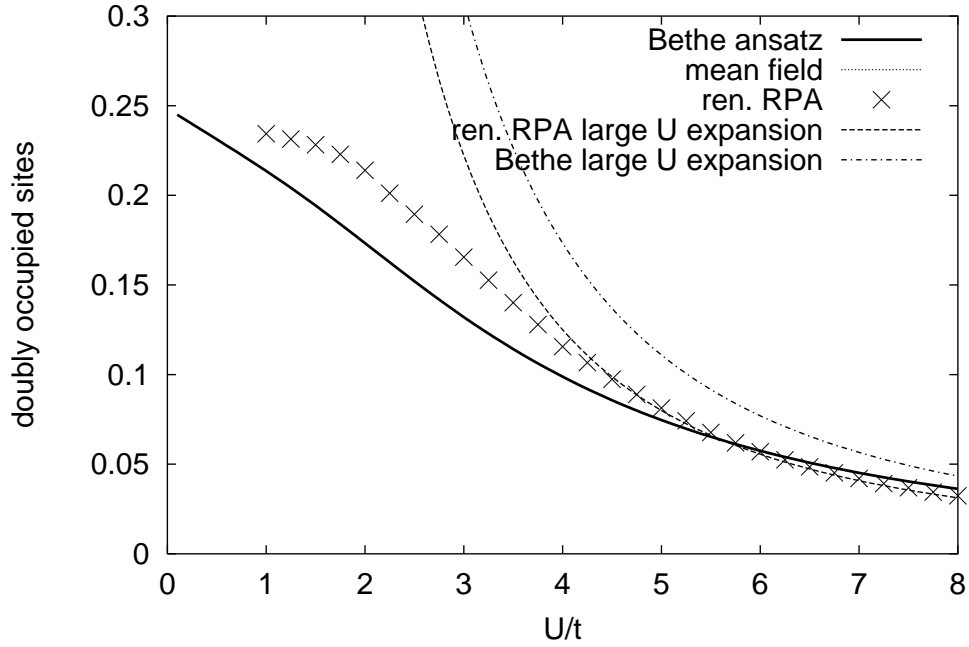


FIG. 18. Number of double occupancies per site for the half filled Hubbard chain.